LBL-12087
Preprint

Lawrence Berkeley Laboratory
UNIVERSITY OF CALIFORNIA, BERKELEY

EARTH SCIENCES DIVISION

Submitted to Water Resources Research

MULTIDIMENSIONAL NUMERICAL SIMULATION OF FLUID FLOW IN FRACTURED POROUS MEDIA

T.N. Narasimhan

February 1980

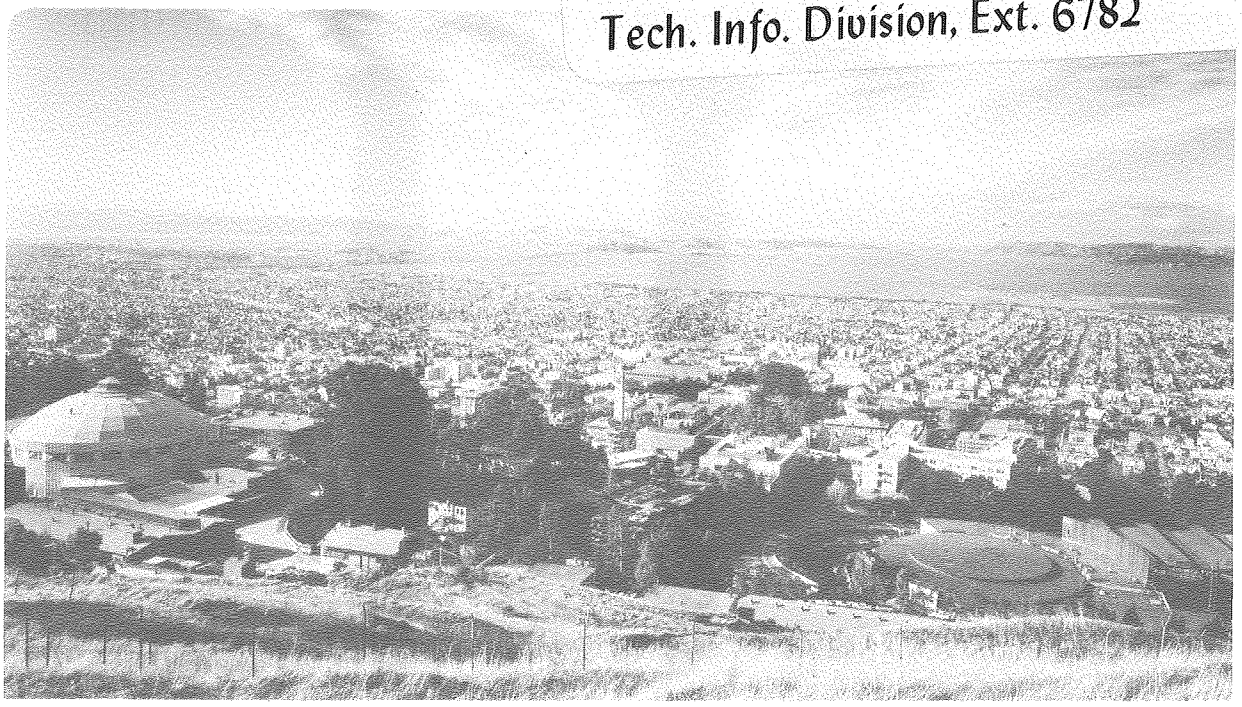

Prepared for the U.S. Department of Energy under Contract W-7405-ENG-48

DISCLAIMER

MULTIDIMENSIONAL NUMERICAL SIMULATION OF FLUID FLOW IN FRACTURED POROUS MEDIA

T. N. Narasimhan
Earth Sciences Division
Lawrence Berkeley Laboratory
University of California
Berkeley, California 94720

ABSTRACT

Fluid flow in fractured porous media can be simulated with considerable ease and generality using an integral finite-difference method (IFDM). The three commonly used conceptualizations of fractured systems, namely, discrete fracture systems, equivalent porous media systems, and double- or composite-porosity systems are all contained within the IFDM formulation. The theoretical basis of the IFDM is briefly described and the method is compared and contrasted with the finite difference and the finite element methods. Six illustrative examples are provided to demonstrate the applicability of the method to fractures, with fixed or variable geometry, to advective-diffusive chemical transport in a fractured system and to a double-porosity system.

INTRODUCTION

At present there is considerable interest in the possibility of disposing of nuclear wastes in extremely low permeability geological environments such as those obtained in igneous and metamorphic rocks or in ancient argillaceous materials. Though lacking in primary porosity, these rocks are known to contain fractures down to several kilometers below land surface. Moreover, the stress-relief accompanying the underground openings and the associated shafts

will also lead to the creation of artificial fractures that may extend to at least a distance of a few shaft or repository diameters. The fractures, which may have apertures as small as 1 to 10 microns, may, over a period of thousands of years, provide pathways for migrating groundwaters from the repository to the biosphere. Long-term acceptability of deep waste-disposal sites is therefore very much dependent on our ability to simulate the evolution of the groundwater regimes in such fractured rock systems.

Approaches to Modeling Fractured Systems

Fractured rock systems of interest in radioactive waste disposal consist of extremely low permeability rocks (10^{-9} to 10^{-4} darcies) intersected by one or more fracture sets. The fractures, whose permeability is directly related to their apertures, provide the main conduits for water movement with some diffusive leakage into the rock matrix. Modeling the flow of water under such conditions involves the simulation of a highly heterogeneous system with complex geometry. Even with the current availability of powerful computers, a detailed handling of such systems requires capabilities of handling enormous quantities of data, not economically feasible at the present time except when the flow region is relatively small (e.g., the region immediately adjoining the repository).

In general, three approaches have been proposed in the literature to handle fractured-porous systems. These are:

1. Equivalent Porous Medium Approach: In this approach, the fractured system is grossly treated as an equivalent non-isotropic statistical continuum.

The tacit assumption is that physical quantities such as potential, porosity, pressure, and so on, are averaged over sufficiently large blocks of rock containing a large number of fractures. Obviously, the sizes of such a representative block will increase with increased fracture spacing. Computations based on this model will, in general, be relevant only to field observations made with measuring devices with large characteristic lengths (e.g. wells with large open intervals). From a practical standpoint, there is general agreement among many workers that the equivalent porosity model is a reasonable method to analyze the fluid flow regime far away from the repository. One of the serious drawbacks of this approach is that there is as yet no well-defined method for computing the gross, porous media parameters, even if the fracture details are completely prescribed. This is because the gross parameters are very much dependent on scale and there is reason to believe that the gross system may in general truly be anisotropic, rather than orthotropic as is commonly assumed in the literature.

2. Double-Porosity Approach: The double-porosity approach was originally proposed by Barenblatt et al., 1960, to analyze flow in fractured-porous media. In this approach, the flow region is mathematically idealized as a complex of two interacting media, one representing the fissured-regime and the other representing the porous regime. The fissured regime is characterized by very high permeability and very low storage while the porous-block regime is characterized by low permeability and high storage. Such a system may be described by two conservation equations, one for each aforesaid regime. These two equations are to be coupled by a fluid transfer term expressed as a nonlinear

source term, dependent on the potential difference between the regimes at the location of interest. This double-porosity model enabled the development of several useful analytical solutions for well-test analysis in the petroleum literature (e.g., Warren and Root, 1963; Odeh, 1965) for naturally fractured reservoirs. The double-porosity approach, or better still, the interacting, double-continuum approach is truly a mathematical approximation whose exact relation to physics is ill-defined. For example, the analytic solution of the double porosity system yields two values for potential at every point in the system, one for the fracture regime and one for the porous regime. How do these quantities relate to the actual physical measurement at the location? Moreover, the source-term which couples the two regimes is proportional to the difference in the two potentials through a coefficient whose physical significance is not well-defined. Yet, when one is not interested in a detailed description of what happens within the reservoir, the above deficiencies can be overlooked and the double porosity system can be used as a practical tool for modeling and prediction. Such indeed is the case when one chooses to use this model for analyzing well-test data from naturally fractured reservoirs.

The utility of the double-porosity model in regard to waste-isolation studies depends on the manner in which the model output is to be utilized. For example, for modeling chemical transport problems, the double-porosity model output will not be reliable since a fairly well-defined fluid flux field is a necessary input for solving the transport equation. Furthermore, it is not clear to this writer that the double-porosity concept is needed at all when one chooses to solve the over-all problem by numerical methods. As we

shall see later, numerical models, developed directly from the basic integral equation, help not only in dispensing with hard-to-define internal boundary conditions, but also provide a great deal of flexibility in modeling any part of the flow region with any desired degree of fineness. Thus, in a numerical model of a fractured medium, the double-porosity model can be treated realistically as a limiting case in which the porous blocks are discretized very coarsely.

3. The Discrete Fracture Approach: In this very general approach, the fractures and the porous matrix are separately discretized into volume elements and the conservation equations are solved for each such volume element. A principal drawback to this approach is the amount of detail that is required as input and the accompanying effort involved in obtaining numerical solutions. Nevertheless, it appears that such a detailed effort is necessary to analyze the flow regime in the vicinity of the underground opening. Also, very little is known at present about the factors that govern the transformation of parameters from one scale to another In order to gain insight into the question of scale transformation, the discrete fracture model is a tool of fundamental necessity.

Purpose and Scope

The purpose of this paper is to present a general, multidimensional numerical model for simulating fluid flow in fractured porous media. The model is inherently sufficiently general to include the three approaches described above as particular cases. Conceptual-theoretical discussions are

provided to develop the problem in an integrated fashion. Some numerical results are presented to substantiate the theoretical arguments. In scope, the paper is restricted to isothermal fluid flow.

THEORY

Conceptual Framework

The basic law of mass conservation is applicable to any elemental volume ℓ of the flow region, whether that elemental volume comprises a portion of a fracture, a portion of the rock matrix, or even a combination of both. According to the law of mass conservation, the algebraic sum of the fluxes crossing the surface enclosing volume element and the arbitrary withdrawal of fluids from ℓ (the sources) equals the rate of change of fluid mass in ℓ, thus,

$$\rho_\ell G_\ell + \int_{\Gamma_\ell} \rho K \vec{\nabla}\phi \cdot \vec{n} d\Gamma = \frac{\partial M_{w,\ell}}{\partial t} \qquad (1)$$

where ρ_ℓ is average fluid density within ℓ; G_ℓ is the volumetric rate of fluid generation from ℓ; ρ is fluid density at $d\Gamma$; K is the hydraulic conductivity at $d\Gamma$; $\phi = z + \psi$ is the fluid potential where z is elevation and ψ is pressure head; $\vec{n}$ is unit outernormal to $d\Gamma$; $M_{w,\ell}$ is the mass of water contained in ℓ and Γ_ℓ is the closed surface bounding the volume element ℓ. Should the system be fully saturated with water, and should the fluid potential vary smoothly over the volume element, then $M_{w,\ell}$ can be related to the average pressure head $\bar{\psi}_\ell$ at an interior nodal point in the system by the relation,

$$M_{w,\ell} = \overset{\circ}{M}_{w,\ell} + (dM_{w,\ell}/d\psi_\ell)\bar{\psi}_\ell \tag{2}$$

and

$$dM_{w,\ell}/d\psi_\ell = V_\ell \rho_\ell S_{s,\ell} \tag{3}$$

where $\overset{\circ}{M}_{w,\ell}$ is the mass content of ℓ at $\bar{\psi}_\ell = 0$, V_ℓ is the volume of ℓ and $S_{s,\ell}$ is the specific storage of the material in ℓ given by

$$S_{s,\ell} = \rho_\ell g(n\beta + m_{v,\ell}) \tag{4}$$

where g is acceleration due to gravity, n is porosity, β is compressibility of water and $m_{v,\ell}$ is the coefficient of volume change (rate of change of bulk volume with external pressure) of the material in element ℓ. Additionally, if we neglect time-dependent changes in elevation of the nodal points due to very small deformations, then, $\Delta\bar{\psi}_\ell = \Delta\bar{\phi}_\ell$. Moreover, Γ_ℓ may either be completely interior to region ($\Gamma_{\ell,m}$) or portions of it may coincide with the external bounding surface of the system ($\Gamma_{\ell,b}$). Hence we may rewrite (1) as

$$\rho_\ell G_\ell + \int_{\Gamma_{\ell,m}} \rho K \vec{\nabla}\phi \Gamma \cdot n d\Gamma + \int_{\Gamma_{\ell,b}} \rho K \vec{\nabla}\phi \cdot n d\Gamma = M_{c,\ell} \frac{\partial \phi_\ell}{\partial t} \tag{5}$$

where $M_{c,\ell} = dM_w/d\psi = \rho_\ell V_\ell S_{s,\ell}$ is the fluid mass capacity of the volume element ℓ, defined as the change in mass of water in ℓ due to a unit change in head under conditions of drainage. In heat-flow problems, the analagous quantity is the heat capacity of an arbitrary mass of material.

The integral representation in (5) may be applied to any volume element, finite or infinitesimal. If one applies (5) to an infinitesimal element and divides both sides through by V_ℓ, the result is the well-known differential expression,

$$\rho_\ell g_\ell + \text{div } K\vec{\nabla}\phi = m_{c,\ell}\left(\frac{\partial \phi_\ell}{\partial t}\right), \tag{6}$$

where g_ℓ is G_ℓ/V_ℓ and $m_{c,\ell} = M_{c,\ell}/V_\ell$.

However, since our purpose is to develop a numerical model and since the numerical approach consists in applying the conservation equation to finite subdomains of the flow region, we may directly proceed from (5) and write down the discretized equations. We will not follow the redundant step of integrating (6) to obtain (5). Note also that in (5) the second integral on the right-hand side incorporates the known boundary conditions either in the form of known ϕ (prescribed potential condition) or in the form of known $k\nabla\phi\cdot\vec{n}$ (prescribed flux condition). That is, (5) imbeds the boundary condition into the conservation statement.

For purposes of numerical computations, if one chooses the volume element to be sufficiently small so that (2) is satisfied at all times with reference to ψ_ℓ measured at the representative nodal point, then one may directly apply (5) to ℓ. Also, if Γ_ℓ and t are divided into a finite number of segments, then, the integrals may be replaced by finite sums and the differentials by finite differences to obtain,

$$\rho_\ell G_\ell + \sum_m \rho_{\ell m} K_{\ell m} (\vec{\nabla}\phi \cdot \vec{n}) \Delta\Gamma_{\ell m} + \sum_b \rho_{\ell b} K_{\ell b} (\vec{\nabla}\phi \cdot \vec{n}) \Delta\Gamma_{\ell b} = M_{c,\ell} \frac{\Delta \phi_\ell}{\Delta t}, \tag{7}$$

in which m denotes all interior surface segments and b denotes all exterior surface segments. Note that (7) applies to any arbitrary volume element and hence it is an invariant statement. As shown in Fig. 1, (7) may be applied

a portion of a fracture or a portion of a porous medium. When (7) is applied to a fracture (Fig. 1B), then, for the segment of Γ_ℓ representing the fracture-rock interface ($\Delta\Gamma_{f,r}$ in Fig. 1B) one has to use $K_{f,r}$ in applying (7) where $K_{f,r}$ is the hydraulic conductivity of the rock-fracture interface. It is of interest to note here that in the double-porosity model, the flux across this surface is treated as a source term included in G_ℓ. This source term is the internal boundary condition linking the fissure regime and the porous regime. Thus, in the double-porosity model, the term ($\rho_\ell K_{\ell m} \vec{\nabla}\phi \cdot n d\vec{\Gamma}$) for the fracture rock interface is replaced by an equivalent term $\rho_\ell \alpha^* K_r(\phi_r - \phi_\ell)$ where ϕ_r is the average potential in the block, ϕ_ℓ is the potential in the fracture, $K_{\ell m} = K_r$ in the matrix hydraulic conductivity and α^* is a function of the surface area of the fracture interface and a characteristic length of the block. As we shall see later, the model described in this paper is flexible enough to handle either of the two methods of handling the fracture rock interface.

It is not difficult to see in this regard that in a rock system with irregular fracture distributions, α^* should vary widely from one location to another in the flow region. Yet the double-porosity model assumes this factor (or a factor α related to α^* by $\alpha = \alpha^*/V$) be constant everywhere in the flow region. Obviously, the double-porosity approach is extremely simplistic for naturally fractured systems. Conversely, estimates of α obtained indirectly from interpretation of well tests can only be model coefficients with very limited use. Application of the α to a detailed modeling of the reservoir can lead to unrealistic estimates of fluid potentials and fluxes over the flow region.

The Chosen Approach

In the present work we shall choose the approach of directly applying (7) to well-defined subdomains of the flow region. Additionally, we shall choose to evaluate the quantity $(\vec{\nabla}\phi \cdot \vec{n})$ at each interface between volume elements by the finite difference approximation

$$\vec{\nabla}\phi \cdot \vec{n}\Big|_{\ell,m} \sim \frac{\phi_m - \phi_\ell}{D_{\ell,m}} \tag{8}$$

where $D_{\ell,m}$ is the distance between the nodal points ℓ and m. Equation (8) presupposes that the line joining ℓ and m coincides with the normal to the interface $\Delta\Gamma_{\ell,m}$. Figure 2 is a sketch of a volume element ℓ of arbitrary shape in the rock matrix which communicates with other rock or fracture elements. In Fig. 2, $D_{\ell,m} = d_{\ell,i} + d_{m,i}$, where $d_{\ell,i}$ and $d_{m,i}$ denote, respectively, perpendicular distances from nodes ℓ and m to the interface $\Delta\Gamma_{\ell,m}$.

This approach has been termed the Integral Finite Difference Method (IFDM; Narasimhan and Witherspoon, 1976) since this method directly evaluates the surface integrals and the associated volume averages and since it uses the finite difference approach for evaluating gradients of potential. This approach, which has been known since the early 50's (MacNeal, 1953; Dusinberre, 1961), was translated into a very powerful computer program called TRUMP by Edwards (1972). Many of the ideas inherent in the following discussions have originated from Edwards.

The discretized IFD equations now become,

$$\rho_\ell G_\ell + \sum_{\substack{m \\ \ell \neq m}} U_{\ell m}(\phi_m - \phi_\ell) + \sum_b U_{\ell b}(\phi_b - \phi_\ell)$$

$$= M_{c,\ell} \frac{\Delta\phi_\ell}{\Delta t} \quad (\ell = 1, 2, 3, \ldots, L) \tag{9}$$

where $U_{\ell,m}$ is the conductance of the interior surface $\Delta\Gamma_{\ell,m}$, given by

$$U_{\ell,m} = \frac{\rho K_{\ell m} \Delta\Gamma_{\ell,m}}{D_{\ell,m}} \tag{10}$$

$U_{\ell,b}$ is the conductance of the external surface segment, $\Delta\Gamma_{\ell,b}$ given by

$$U_{\ell,b} = \frac{\rho K_\ell \Delta\Gamma_{\ell,b}}{D_{\ell,b}} \tag{11}$$

L is the total number of nodes in the flow region for which $\Delta\phi_\ell$ is to be computed and m denotes a volume element having an interface with volume element ℓ. Rearranging terms in (9), we get

$$\rho_\ell G_\ell - \phi_\ell \left[\sum_m U_{\ell,m} + \sum_b U_{\ell,b}\right] + \sum_m U_{\ell,m}\phi_m + \sum_b U_{\ell,b}\phi_b$$

$$= M_{c,\ell} \frac{\Delta\phi_\ell}{\Delta t} \tag{12}$$

Equations (9) and (12) are central to the IFDM. Apart from the source terms and the material properties, a key task in the IFDM is to provide the geometric quantities $D_{\ell m}$, $\Delta\Gamma_{\ell,m}$ and V_ℓ that are needed to evaluate $U_{\ell,m}$, $U_{\ell,b}$ and $M_{c,\ell}$. In the IFDM these quantities are provided directly as input, for each interface and volume element in the flow region. Equation (9) is in a form very

convenient for writing the iterative procedure used in the computer program TRUMP, and its derivatives while (12) is convenient to express the equation in a global matrix form for direct solution purposes. We shall return to (12) later when comparing IFDM with other methods.

Marching in the Time Domain

In (9) ϕ_m and ϕ_ℓ are both functions of Δt and we have to use appropriate mean values, $\bar{\phi}_m$ and $\bar{\phi}_\ell$ such that

$$U_{\ell m}(\bar{\phi}_m - \bar{\phi}_\ell) = \int_{t_o}^{t_o+\Delta t} U_{\ell,m}(\phi_m - \phi_\ell)dt \tag{13}$$

and

$$U_{\ell b}(\bar{\phi}_b - \bar{\phi}_\ell) = \int_{t_o}^{t+\Delta t_o} U_{\ell,b}(\phi_b - \phi_\ell)dt \tag{14}$$

To achieve this (Narasimhan et al., 1978, Edwards, 1972), express these mean values by

$$\bar{\phi}_\ell = \phi_\ell^\circ + \lambda\Delta\phi_\ell \tag{15}$$

$$\bar{\phi}_m = \phi_m^\circ + \lambda\Delta\phi_m \tag{16}$$

where ϕ_ℓ° and ϕ_m° are the initial values corresponding to time t_o and $0 \leqslant \lambda \leqslant 1$ is a weighting factor. For $\lambda = 0$, leads to a set of explicit expressions for the $\Delta\phi$'s. However, the explicit expression for any element ℓ will violate maximum principle when Δt exceeds the critical time constant for the element. This critical value, called a stable time-step, is the ratio of capacity of ℓ

to the sum of its surface conductance,

$$\Delta t_{stab,\ell} = \frac{M_{c,\ell}}{\sum_{m} U_{\ell,m} + \sum_{b} U_{\ell,b}} \tag{17}$$

for a stable solution, therefore, when $\Delta t > \Delta t_{stab,p}$, we substitute (15) and (16) into (9) to arrive at an implicit set of equations (simultaneous equations). For convenience, we rearrange terms to express $\Delta\phi_{\ell}$ in terms of an explicit part and an implicit part. Thus,

$$\Delta\varphi_{\ell,explicit} + \frac{\lambda\Delta t}{M_{c,\ell}} \left\{ - \sum_{b} U_{\ell,b}\Delta\phi_{\ell} + \sum_{m} U_{\ell m}(\Delta\phi_{m} - \Delta\phi_{\ell}) \right\} = \Delta\phi_{\ell} \tag{18}$$

where

$$\Delta\phi_{\ell,explicit} = \frac{\Delta t}{M_{c,\ell}} \left\{ \rho_{\ell} G_{\ell} + \sum_{m} U_{\ell,m}(\phi^{\circ}_{m} - \phi^{\circ}_{\ell}) + \sum_{b} U_{\ell,b}(\phi_{b} - \phi^{\circ}_{\ell}) \right\} \tag{19}$$

We now reason that we could first compute the $\Delta\phi_{\ell,explicit}$ values for every ℓ in the flow region and then evaluate the second quantity on the left-hand side of (18) only for those ℓ for which $\Delta t > \Delta t_{stab,\ell}$. This has been called the mixed explicit-implicit approach. In applying (18) thus, if, for a given ℓ and m

$$\Delta t > \Delta t_{stab,\ell} \quad \text{but } \Delta t < \Delta t_{stab,m}$$

then, we replace

$$U_{\ell,m}(\Delta\phi_{m} - \Delta\phi_{\ell}) \text{ by } U_{\ell,m}(\Delta\phi_{m,explicit} - \Delta\phi_{\ell}).$$

The mixed explicit-implicit approach thus does the implicit calculations only in those parts of the flow region where stability is violated. In other words, if isolated areas of instability are separated in a flow region by areas of

stability, then the unstable regions are essentially decoupled from one another within each time step. Under these circumstances, the mixed explicit-implicit strategy helps us to partition the large global matrix and obtain solution by solving several small submatrices. For details of this strategy see Edwards (1972), Narasimhan et al (1978), and Neuman and Narasimhan (1977).

Computer Programs

The basic IFD model was originally developed by Edwards (1972) for heat transport with conduction, convection, and radiation and incorporated into a program called TRUMP. Subsequently, this model was adapted at the Lawrence Berkeley Laboratory to solve porous media fluid flow problems. These programs include: TRUST, for solving saturated-unsaturated flow in deformable media (Narasimhan et al., 1978); TERZAGI, for saturated flow in deformable media; CCC, for heat and water transport in deformable media (Lippmann et al., 1977); and SHAFT79, for two-phase transient flow of heat and mass (Pruess et al., 1979). The discussions that follow in regard to simulating fractures are applicable to all the aforesaid programs subject to suitable modifications. However, the actual applications that follow have been carried out with TERZAGI, except for one case analyzed with TRUMP.

Simulation of Fractured Rock Systems

We have already stated that there are three different ways in which fractured rock systems can be simulated. These include: systems with discrete fractures; double-porosity systems; and equivalent porous media systems. The last of these does not require any further attention since literature is voluminous on modeling porous systems. We will now consider the first two cases.

Systems with discrete fractures: In modeling a porous medium with discrete fractures with the IFDM, we recognize that (9) or (12) are very general in nature and can be applied to an elemental volume, either in a fracture or in the rock matrix, as in Fig. 2. Computationally, a major difference between a matrix element and a fracture element is that the former is usually characterized by higher capacities ($M_{c,\ell}$) and lower hydraulic conductivities and hence large time constants. The latter, on the other hand, are usually characterized by very low capacities and very high hydraulic conductivities and hence very small time constants.

Note from (9) or (12) that in setting up the simultaneous equations, the quantities needing greatest attention in computation are the conductances $U_{\ell,m}$ and $U_{\ell,b}$, since $\rho_\ell G_\ell$ and $M_{c,\ell}$ are directly provided as input. For computing the conductances proper, equations (10) and (11) one needs the hydraulic conductivity at the interface $K_{\ell,m}$, the distance between nodal points $D_{\ell,m}$, and the surface area $\Delta\Gamma_{\ell,m}$. In particular, handling the conductance between a fracture and a matrix element is worth discussing. Because of the much higher hydraulic conductivity of the fractures, the potential gradients along the fracture will be relatively small compared to that within the block and hence, a single fracture element may be connected to one or more rock elements along a given fracture surface. Moreover, since the gradient of potential across the fracture opening can be neglected, the fracture rock conductance, $U_{f,r}$, is is determined by

$$U_{f,r} = \frac{\rho K_r \Delta\Gamma_{f,r}}{d_{r,i}}$$

where K_r is the hydraulic conductivity of the rock matrix, $\Delta\Gamma_{f,r}$ is the interface area and $d_{r,i}$ is the distance from the nodal point of the rock element to the interface $\Delta\Gamma_{f,r}$.

It is now appropriate to discuss the fracture parameters. Insofar as adjoining fracture elements are concerned, we need to use the hydraulic conductivity of the fracture, K_f in computing conductance. It is now well established that K_f is related to 2b, the fracture aperture. Experimental evidence (Witherspoon et al., 1980) suggests that laminar fluid flow in a fracture can be very closely approximated by the relation,

$$Q_f = \frac{(2b)^2 \rho g}{12\mu} \cdot (2b\Delta\ell_f) \cdot \frac{\partial\phi}{\partial x} \tag{21}$$

where Q_f is the flux in the x direction, 2b is the fracture aperture, μ is the coefficient of viscosity and $\Delta\ell_f$ is the length of the fracture trace on the plane across which Q_f is measured. For the sake of a definition, if we let $\Delta\ell_f = 1$ and $\partial\phi/\partial x = 1$, then, $Q_f = (2b)^3\rho g/12\mu$. Hence the expression "cubic law" is used to characterize fluid flow in fractures. Realistically, therefore, we could define the fracture hydraulic conductivity to be

$$K_f = \frac{(2b)^2 \rho g}{12\mu} \tag{22}$$

Finally, we discuss the meaning of the storage parameter for a fracture element. For a fracture element ℓ, if we neglect the compressibility of the rock grains, the quantity of water released from storage per unit change in pressure head is given by

$$M_{c,\ell} = \frac{d(V_{v,f}\rho)}{d\psi} = V_{v,f}\frac{d\rho}{d\psi} + \rho\frac{dV_{v,f}}{d\psi} \tag{23}$$

where $V_{v,f}$ is the volume of voids in the fracture element ℓ. However, for convenience, we may normalize $V_{v,f}$ with reference either to bulk volume $V_{b,f}$ or solid volume $V_{s,f}$ of the fracture element. If we are to normalize (23) with reference to $V_{b,f}$ and recognize that $p = \rho g \psi$, where p is pressure, we obtain,

$$M_{c,\ell} = V_{b,f}\, \rho g[n_f \beta + m_{v,f}] \tag{24}$$

where $n_f = V_{v,f}/V_{b,f}$ is "porosity" of the fracture element and $m_{v,f} = -dn/dp$ is the coefficient of volume change [Lambe and Whitman, 1969] of the fracture element.

Or, as has been done is TERZAGI in which the volume element is always defined as having the same volume of incompressible solids, it is more convenient to normalize (23) with reference to $V_{s,f}$. Thus,

$$M_{c,\ell} = V_{s,f}\rho g[e_f \beta + a_{v,f}] \tag{25}$$

where e_f is the void ratio of the fracture and $a_{v,f} = -de_f/dp$ is the coefficient of compressibility for the fracture. Note that whether one uses V_b with n and m_v, or one uses V_s with e and a_v, the final quantity $M_{c,\ell}$ is the same as long as one is consistent.

We note here that in the case of a volume element in a fracture, the element itself is made only of the voids. However, for convenience we may associate any arbitrary solid volume $V_{s,f}$ with the fracture and define a fictitious bulk volume $V_{b,f} = V_{s,f} + V_{v,f}$ for the fracture element. Since $V_{s,f}$ is is arbitrarily chosen, we can, in fact choose it in such a fashion that e_f becomes exactly equal to 2b, the fracture aperture. This can be achieved by letting $V_{s,f} = A_f$ times unit thickness, where A_f is the surface area of the

fracture wall. In this case,

$$e_f = \frac{(A_f)(2b)}{A_f(1)} = 2b \tag{26}$$

If we use this procedure for $a_{v,f}$ in (25) we may use experimental data directly on fracture closure as a function of stress, i.e., $a_{v,f} = -d(2b)/dp$.

It is apparent from the foregoing that once we have defined the appropriate conductances for fracture-fracture, fracture-rock and rock-rock interfaces and have defined the physically appropriate storage parameters for volume elements in the fracture or in the rock, the solution of the discrete fracture problem merely reduces to solving (9) or (12) through direct or iterative techniques.

Systems idealized by double porosity: In the double porosity approach all the fractures are idealized into one continuum and all matrix blocks into another. For an intersecting system of fractures the physical significance of the fracture continuum is difficult to comprehend. For purposes of elucidation, therefore, it is best to discuss the relation of the double porosity model to a simple idealized system of horizontal fractures as shown in Fig. 3. Consider a system of I horizontal fractures with spacing S. The thickness, H, of this system is given by H = IS. It is clear that in this system water moves horizontally in the fractures and water drains vertically from the intervening blocks to the fractures bounding the matrix. The system is bounded above and below by impermeable boundaries. We will now replace this system by two interacting continua, each of thickness H, one representing the flow phenomenon in

the fractured milieu and the other, that in the matrix milieu. Obviously, the fracture continuum is characterized only by horizontal flows while the matrix continuum only by vertical flows.

If we assume that flow in the fracture obeys the cubic law, then the total horizontal flux in the horizontal direction in the layer equals I times the flux in each fracture. We may therefore define the average hydraulic conductivity, K_f^*, of the fracture continuum by,

$$K_f^* = \frac{I(2b)^3 \rho g}{12\mu H} \tag{27}$$

Similarly if $S_{s,f}$ is the storativity for one fracture, then, $S_{s,f}^*$, the average storativity, for the fracture continuum is,

$$S_{s,f}^* = \frac{I(S_{s,f}(2b))}{H} \tag{28}$$

Since the fracture aperture is far smaller than the fracture spacing, $K_r^* \approx K_r$ and $S_{s,r}^* = S_{s,r}$, where K_r^* and $S_{s,r}^*$ are the average hydraulic conductivities and storativities of the rock continuum.

Consider an area A_f at the interface between a fracture and an adjoining matrix block. The flux from the block to the fracture is given by

$$Q_{f,r} = \frac{K_r A_f}{0.5S} (\phi_r^* - \phi_f^*) \tag{29}$$

and the total flux from blocks to fractures is given by $2IQ_{f,r}$. In (29), ϕ_r^* and ϕ_f^* are average potentials in the element of each continuum.

If we consider two volume elements at a given location, one in the fracture continuum and one in the porous continuum, each element having an area of cross section A_f and height H, then $V_f^* = V_m^* = A_f H$. It is assumed, in formulating the differential equations of the double porosity model, that the two volume elements of identical bulk volume are centered at the same location in space. For each of these volume elements we may now write a conservation equation.

Fracture continuum element

$$\int_\Gamma (\rho K_f^* \nabla \phi_f^* \cdot \vec{n} d\Gamma) + \frac{2\rho I K_r A_f}{0.5S} \cdot (\phi_r^* - \phi_f^*) = \rho V_f^* S_{s_f}^* \frac{\partial \phi_f^*}{\partial t} \tag{30}$$

Rock continuum element

$$\frac{-2\rho I K_r}{0.5S} A_f (\phi_r^* - \phi_f^*) = \rho V_r^* S_{s_r} \frac{\partial \phi_r^*}{\partial t} \tag{31}$$

Noting that $V_r^* = V_f^* = A_f H$ and dividing through by V_f^* in (30) and V_r^* in (31) and letting the elements tend to zero is the limit, we now obtain the differential equation,

$$-\text{div } \rho K_f^* \vec{\nabla} \phi_f^* + \rho \alpha K_r^* (\phi_r^* - \phi_f^*) = \rho S_{s,f}^* \frac{\partial \phi_f^*}{\partial t} \tag{32}$$

$$-\rho \alpha K_r^* (\phi_r^* - \phi_f^*) = \rho S_{s,r}^* \frac{\partial \phi_r^*}{\partial t} \tag{33}$$

where

$$\alpha = \frac{2I}{0.5SH} = \frac{4}{S^2} .$$

since H = IS. Obviously α is a factor controlled by the spacing and the specific surface of the rock blocks. Note also that in the fracture continuum water flows within the continuum as well as across an imaginary interface with the rock continuum. Hence, (32) has a source term as well as a divergence term on the left hand side. However, it is assumed that, due to the strong permeability contrast between the fracture and the blocks, flow of water within the blocks is restricted to lines normal to fracture-block interfaces. Hence, in (32) the divergence term is absent.

In view of (30) and (31) we may now proceed to apply (9) to a double-porosity system. First, we discretize the flow region into ℓ = 1, 2, 3, ... L subdomains to represent the elements of the fracture continuum with K_f^* and $S_{s,f}^*$ defined as in (27) and (28). For each of these subdomains we shall provide all required input data such as G_ℓ, interior connection data, exterior connection data and bulk volumes so that one equation such as (9) can be developed for each of the L elements. Simultaneously we assume that at the location of each ℓ = 1,2,3,...L fracture continuum element there exists a matrix continuum element j = 1, 2, 3, ... L such that $V_\ell = V_j$ for $\ell = j$. In order to couple the two continua we will now connect, for each $\ell = j$, the fracture continuum element ℓ with the matrix continuum element j in such a fashion that the conductance $U_{\ell,j}$ is given by,

$$U_{\ell,j} = \frac{I\rho K_r^* \Delta\Gamma_{\ell,j}}{d_{j,i}} = \frac{I\rho K_r^* A_f}{0.5S} = \rho V_r \alpha K_r^* \tag{34}$$

We thus end up with conservation equations for 2L volume elements in all, with one equation for each fracture-continuum and matrix-continuum element. Note that the time-constant for the respective elements shall be given by

$$\Delta t_{stab,\ell} = \frac{V_f S^*_{s,f}}{\sum_m U_{\ell,m} + \sum_j U_{\ell,j}} \tag{35}$$

where ℓ, m are fracture continuum elements, j is a matrix continuum element, and $j = \ell$; and

$$\Delta t_{stab,j} = \frac{V_r S^*_{s,r}}{2U_{\ell,j}} \tag{36}$$

where j is a fracture continuum elements, ℓ is a matrix continuum element, and $j = \ell$.

Since the IFDM is so structured that the geometric quantities ($\Delta\Gamma_{\ell,m}$ and $D_{\ell,m}$) needed for computing the conductances are directly provided as input data, the handling of $V_r\alpha$ needed as input for computing $U_{\ell,j}$ in (34) poses no special problem. Also, since the 2L simultaneous equations are formulated, they can be solved by the mixed explicit-implicit method. Indeed, since the double-porosity model gives rise to a stiff matrix (due to the marked differences in the time-constants between the fracture-continuum elements and the matrix-continuum elements), the mixed explicit-implicit method is particularly desirable for solution.

Comparison of IFDM with Other Approaches

Having described the utility of the IFD approach to handle a variety of fracture-simulation problems, it is of interest to see how this approach compares with other numerical techniques, notably, the conventional finite difference method (FDM) and the finite element method (FEM).

IFDM and FDM: The basic difference between these two approaches is that the latter is applied specifically to volume elements with faces perpendicular to the coordinate axes while the former is applied in general to arbitrarily shape elements. The reason for this is that the FDM seeks to directly approximate the partial differential equation, which includes second derivatives of potential in space. Note that the partial differential equation expresses the conservation law per unit volume of the volume element. This volume normalization, coupled with the regular shape of the volume element helps obtain the second derivatives in space. The IFDM, however, chooses not to use the volume-normalization procedure and expresses the conservation law for an arbitrary volume element. Yet, if one applies the IFDM to a mesh involving regularly-shaped volume elements, then the IFDM and FDM equations shall be identical except for division by the bulk volume. Thus, the FDM may be treated as a limiting case of the IFDM.

IFDM and the FEM: The conceptual similarity between these two techniques lie in the fact that both are integral methods in which intensive properties such as potential are expressed as averages over finite volume elements. However, these two methods differ (a) in the manner of carrying out integration

operations and (b) in the approach employed for evaluating gradients of potentials. In order to compare the integration procedures adopted in the IFDM and the FEM, it is instructive to recall equations (9) and (12) that are central to the IFDM. For convenience, we may write (12) in matrix notation as

$$\sum_{m=1}^{L} A_{\ell m}\, \phi_m - \rho_\ell V_\ell S_{s,\ell}\, \frac{\Delta\phi_\ell}{\Delta t} = B_\ell \qquad (37)$$

where

$$A_{\ell,\ell} = \left\{ \sum_m U_{\ell m} + \sum_m U_{\ell b} \right\}$$

$$A_{\ell,m} = U_{\ell,m}$$

and

$$B_\ell = -\left[\rho_\ell G_\ell + \sum_b U_{\ell,b}\phi_b \right]$$

In (37) the $A_{\ell,m}$'s denote the conductances between elements ℓ and m. If an element ℓ communicates with an element m across some common interface then $A_{\ell,m} \neq 0$. Or else $A_{\ell,m} = 0$. Also, ρ_ℓ, V_ℓ, S_s, ℓ and B_p are known, while ϕ_m is a function of initial conditions and the $\Delta\phi_\ell$ is the variable to be solved for. In setting up (37) a major task is to evaluate the coefficients $A_{\ell,m}$ and V_ℓ in order to set up the equations. Note that $A_{\ell,m}$ includes in itself certain geometric quantities in addition to the material properties. In the handling of the geometric quantities inherent in $A_{\ell,m}$ IFDM and FEM choose different approaches. Thus, the IFDM explicitly defines each volume element by defining its bounding surface segments and directly provides the required geometric inputs $\Delta\Gamma_{\ell,m}$ and $D_{\ell,m}$ required for computing $A_{\ell,m}$. On the other

hand, the FEM, as it is commonly employed, chooses an indirect approach to achieve the same purpose. In the FEM, the geometric inputs consist of the coordinates of the nodal points as well as a description of the connectivity between specific nodal points. From this information the geometric quantities inherent in $A_{\ell,m}$ are generated through a process of weighted volume integration. A consequence of this approach is that one avoids the need to explicitly describe the surface segments $\Delta\Gamma_{\ell,m}$ between communicative volume elements. The volume elements are implicitly described, as it were. While this appears to be desirable in that one bypasses the need quantitatively for describing surface segments, the volume integration leads to a different type of computational requirement. That is, the volume integration requires the differential volume element of integration dV to have a simple geometrical shape such as a triangle, a rectangle, a toroid, a tetrahedron, or a parallelipiped. As a result, the integration in the volume integral has to be expressed with reference to a specific coordinate system. In comparison, the IFDM evaluates each conductance term locally in a single one-dimensional form and hence is independent of any coordinate system. Thus, an important difference between the FEM and the IFDM is that in the former conductances are computed through a process of volume integration, while in the latter the conductances are computed directly as a product of the required input data. While it would appear that the latter may require greater input effort, it must be stated that an ability to directly prescribe conductances in a simple fashion is extremely helpful in handling certain special cases. For example, such an ability is of help in connecting a well or a single-fracture element to several matrix elements.

Although one could handle this with the finite element method (Narasimhan et al., 1978) there is an extra effort involved in implementing this with the FEM. Moreover, one could argue that by following the IFDM approach one essentially removes the geometric aspects from the mainstream of calculations and in, certain cases, the geometric quantities could be computed with any desired degree of precision before one sets out to solve the conservation equations.

Apart from the integration aspect, the major difference between the IFDM and the FEM consists in the manner in which spatial gradients of potential are evaluated. In fact, it is in regard to this that one should really exercise judgement in choosing between the IFDM and the FEM for handling any given class of problems. As discussed by Narasimhan and Witherspoon (1976), the IFDM employs a simple finite difference approximation for measuring gradients. This demands that for measuring gradient along any given direction, one simply computes the slope in that direction. It follows that the finite difference approximation is capable of giving only one gradient measurement at a time.

Instead, in the FEM, an equation is set up for the variation potential within a region bounded by 3 or more nodal points and gradients are evaluated at any point and in any given direction by partially differentiating the surface fitting the potential variation. Herein lies the unique power of the FEM, which is especially useful when application of Darcy's law at an arbitrarily oriented surface in an anisotropic medium requires gradient of potential in more than one direction. Even here one could argue that one could interpolate the required additional gradients from associated finite difference gradients.

However, an added advantage of the finite element approach is that by choosing a sufficiently large number of nodal points to fit the equation of the variation in potential, one could effectively introduce higher order terms in the expression for gradient, presumably increasing the accuracy of the evaluated gradients. Whether these higher order terms (which, incidentally lead to increased computational effort) lead ultimately to highly accurate solutions in all cases has not yet been firmly established, particularly for transient problems.

In summary, therefore, the differences between the IFDM and the FEM are limited to certain methods of implementing geometric operations. Awareness of these differences show that each of these methods offer unique flexibility and power to handle certain classes of problems. Both of them, used properly, can give results of comparable accuracy. For systems with isotropic materials or with very general three-dimensional configurations, the IFDM provides a model capable of handling complex geometries and variations in symmetry within the flow region. For systems with arbitrarily varying anisotropy or systems in which the mesh deforms in time, the FEM provides flexibility of computations. Indeed, it is possible, in principle, to combine these two methods of handling geometry into a well-organized, single computer program so that within the same flow region each method could be employed as needed for maximum efficiency.

A BRIEF DESCRIPTION OF PROGRAM TERZAGI

Before proceeding to substantiate the preceding theoretical discussions with illustrative examples, it is pertinent here to briefly describe the input organization of program TERZAGI. The input data of this one-, two-, or three-dimensional IFD program is organized into blocks, each block handling one category of information: control parameters (Block 1); material properties (Block 2); fluid properties (Block 3); volume element geometries (Block 4); internal surface connections (Block 5); external surface connections (Block 6); boundary potentials (Block 7); variable sources (Block 8); and initial conditions, constant sources and preconsolidation pressures (Block 9). While a detailed description of the program is out of place here, the following aspects should prove to be of interest to the reader:

o The solution is started with a small time-step and the time-step is increased gradually by not more than a factor of 2 at a time, depending on the progress of solution. Should the convergence be slow or the nonlinear parameters change too rapidly, the time-step is automatically cut down. If desired, the time-step can be manually controlled.

o The implicit solution process is achieved by a point-iterative scheme with an acceleration factor. The implicit weighing factor λ is varied during the solution from 0.57 to 1 depending on the maximum rate of change of potential, in order to minimize time integration errors. Options are available to override this by using forward-, central- or backward differencing modes.

o The required material properties include void ratio, effective stress, coefficient of compressibility, preconsolidation stress, absolute permeability, specific storage, etc. Some of this data could be mutually exclusive. The required fluid properties include fluid viscosity, density, and compressibility.

o The required volume element properties include bulk volume, type of material contained, and average elevation.

o The required data for interior surface connections include the nodal point designations on either side of the interface, the distance between the nodal points, and the magnitude of the surface area.

o Material properties as well as boundary potentials and sources can all be functions of time or potential.

o The model uses the simple effective stress principle that change in effective stress is equal and opposite in sign to change in pore pressure.

APPLICATION TO SOME FRACTURED SYSTEMS

We will now present some illustrative examples on the application of the IFDM to simulate fluid flow in fractured media. The list of these examples is as follows:

Porous Medium with Discrete Fractures: (1) Flow to a well intercepting a single horizontal fracture; (2) Flow to a well intercepting a single vertical fracture; (3) Pulse test in a well intercepting an inclined fracture; (4) Simulation of a hydraulic fracturing experiment; (5) Advective-diffusive transport in a fractured system with spherical particles.

Double Porosity Medium: (6) Flow to a well intercepting a system of horizontal fractures separated by porous blocks.

1. Flow to a well intercepting a single horizontal fracture. Consider a well of finite radius, r_w, fully piercing an aquifer with a horizontal fracture of radius r_f and width w (=2b). The well pumps at a constant rate Q, starting with hydrostatic initial conditions. The problem is to predict the evolution of fluid potential around the well. Gringarten and Ramey (1974) solved this problem analytically and obtained a solution assuming that the fracture is infinitely conducting and that the rate of flux is constant throughout the fracture. Furthermore, the presence of the well was ignored and the fracture was considered to be a discoidal source.

Bodvarsson and Narasimhan (manuscript under preparation) have studied a class of well-flow problems involving a horizontal fracture. The geometry of the system studied by them is given in Fig. 4. As a first step in their study they solved the problem of Gringarten and Ramey using the IFDM program TERZAGI. A comparison of their results with the analytic solution are presented (Fig. 5) in terms of the dimensionless time $T_{D_f} = K_r t/S_{s,r}r^2$ and dimensionless fracture pressure $P_D = (2\pi Krh\Delta\phi)/Q$, where K_r is the hydraulic conductivity of the aquifer, h is the aquifer thickness, $S_{s,r}$ is specific storage of the aquifer, and $\Delta\phi$ is the drawdown is potential in the fracture. As may be seen the agreement is excellent.

In a series of subsequent runs, the study was extended to finite-conductivity fractures in the presence of a realistic wellbore, within which

fluid level changes with fluid production. The results of the studies (for which no analytical solution is available) is given in Fig. 6 in the form of a set of type curves.

2. Flow to a well intercepting a single vertical fracture. Narasimhan and Palen (1979) studied the problem of fluid flow to a well intercepting a single vertical fracture using the program TERZAGI. Both the well and the fracture fully pierce the aquifer. The geometry of the problem is given in Fig. 7. Analytical solutions have been presented in the literature for infinite conductivity (Gringarten et al., 1974) as well as for finite conductivity vertical fractures (Cinco-Ley et al., 1978). To validate their numerical model, Narasimhan and Palen used a mesh as given in Fig. 8. As shown in Fig. 9, they obtained excellent agreement with the analytical results of Cinco-Ley et al. (1978). The small departures for early time results for $C_r = 1$ and $C_r = 0.2$ are primarily due to wellbore storage effects, not considered in the analytical solution. The small departures for $T_{Df} > 8 \times 10^2$ observed with $C_r = 0.2$ or $C_r = 1.0$ are due to the closed external boundaries simulated in the numerical model.

The numerical model is especially suited for simulating deformable fractures for which fracture permeability varies with fracture aperture. This problem is somewhat difficult to handle analytically due to the nonlinearity involved. The results of four cases of flow within a deformable fracture are presented in Fig. 10.

In Fig. 10, Curve 1 relates to a deformable fracture with an initial aperture w = 1 mm and X_f = 10 m. The fracture deformability, quantified by $a_{v,f} = -de_f/dp = -d(2b)/d_p$, is assumed to be 3.28 x 10^{-10} $pascal^{-1}$ and fracture permeability is allowed to vary with aperture according to the cubic law. We will use this curve to be the standard against which we shall compare the remaining three cases.

Curve 2 represents the case in which all factors are the same as in Curve 1, but K_f is assumed to be constant, corresponding to the initial aperture of 1 mm and independent of fracture aperture. As one would expect, Curve 2 shows lesser values of P_D then Curve 1. Curve 3 incorporates the effect of a 0.1 m-radius well into the problem relating to Curve 1. The unit slope for $T_{Df} < 0.2$ represents withdrawal of fluid from storage. As is to be expected, for $T_{Df} \geq 10$, Curve 3 tends to merge gradually with Curve 1.

Curve 4 relates to a problem which was designed to study the effect of fracture compressibility on the pressure transient. In this case the fracture compressibility, $a_{v,f}$, was increased by 48 per cent from 3.28 x 10^{-10} Pa^{-1}. As seen from the figure, this solution begins to depart makedly from Curve 1 for $T_{Df} > 1.0$. The results show that the pressure transient is extremely sensitive to fracture compressibility of deformable fractures.

3. Pulse-test in a well intercepting an inclined fracture. For studying transient fluid flow in tight fractures, the method of pulse-testing is of interest (Wang et al., 1978). Unlike the conventional well test, the pulse test consists in packing of an interval of the formation, charging the well

with a pulse of water at a pressure higher than the formation pressure and letting the pressure decay in the well as a function of time. Analytic solution to this problem with respect to a horizontal fracture in a tight rock has been discussed by Wang et al. Sirisak Juprasert (1979; personal communication) numerically studied the pulse-test problem for an inclined fracture using program TERZAGI. A major effort in this regard was to develop an IFDM mesh with associated geometric quantities. As shown in Fig. 11, the fracture plane is divided into a number of volume elements with the elements assuming radial shapes close to the well. In the immediate vicinity of the well elliptically shaped volume elements were designed to account for the fact that the well pierces the fracture plane in an oblique fashion. Using the mesh shown in Fig. 11, a number of runs were made with various fracture inclinations. Results from three of these runs are presented in Fig. 12. The results indicate that with higher fracture inclination, the pressure pulse dissipates faster in the wellbore. Conversely, if one were to match data from an inclined fracture system against the horizontal fracture solution, one would overestimate the hydraulic conductivity of the fracture.

4. Simulation of a hydraulic fracturing experiment. Since the late 1950's hydraulic fracturing of in situ rocks has been extensively used to stimulate oil and gas reservoirs through the creation of massive hydraulic fractures extending up to several hundred meters from the stimulated well. On a smaller scale, hydraulic fracturing experiments are also used to determine in situ rock stresses (e.g. Haimson and Fairhurst, 1970).

Palen (1980) adapted the TERZAGI model to analyze the pressure transient data from a hydraulic fracturing experiment in granite and to estimate the in situ stresses as well as the fracture parameters. The experiment was conducted at Monticello in South Carolina by the U. S. Geological Survey (Zoback, pers. com, 1979). The hydraulic fracturing was performed at a depth of approximately 300 m below surface over an interval 3 m. An oil-water mixture with a viscosity of 2.35×10^{-3} kg/m.sec (2.35 cp) was used as the injecting fluid. The well was of 0.1524 m (6 inches) diameter and communicated with surface injection equipment through a .0508 m (2.0 inches) diameter tubing. The actual experiment consisted of several injection cycles separating shut-in and bleed-off periods. For illustrative purposes, the observed injection rates and injection pressures are given in Fig. 13.

Numerical simulation of the hydraulic fracturing process requires the modeling of the energy build-up in the well itself, prior to the initiation of the fractures as well as the propagation of the fracture with time. The former aspect requires the treatment of the well as a volume element of the flow region and the latter requires an ability to handle time-dependent geometry, based on fracture extension. While the wellbore aspect is quite easily handled in the standard IFD formulation, appropriate criteria had to be incorporated into the algorithms to extend the fracture. Palen (1980) used two criteria to extend the fractures; (a) that the fluid pressure near the tip of the fracture be in excess of the least principal stress in the horizontal plane and (b) there be enough potential energy in the system to create new fracture surface to overcome the strength of the rock at the fracture tip.

Assuming the fracture to grow in the shape of a "penny", and by adjusting initial fracture aperture, fracture compressibility, minimum in situ stress, and fracture toughness, the fit given in Fig. 14 was obtained. Independent estimates by Zoback (pers. com., 1979) suggests that the minimum principal stress estimated in the simulation closely matched Zoback's estimate.

5. Advective-diffusive transport in a fractured system with spherical particles. We shall now consider a general problem in which flow in the fracture as well as that in the rock matrix is considered in detail. Rather than the diffusion equation which has been of concern so far, we shall now consider an advective-diffusion problem.

Consider a set of parallel, uniform fractures separated by a distance S (Fig. 15). Water enters this semi-infinite region through the fracture at $Z = 0$, at a constant velocity, V_f, and with a solute concentration $C(Z = 0,t) = C_0 e^{-\lambda_d t}$ where λ_d is a decay constant. The solute is transported by advection and longitudinal dispersion, D_L, within the fracture and by diffusion perpendicular to the fracture interface into the rock matrix. Rasmuson and Neretnieks (1980) studied this problem analytically by assuming the rock blocks to be replaced by spherical particles of the same surface to volume ratio. The problem then can be expressed by two partial diferential equations, one for advective-dispersion in the fracture, the other for radial diffusion into the spheres. These two are coupled by the transfer of solute between the fracture and the sphere and are subject to the boundary condition, $C(Z = 0,t) = C_0 e^{-\lambda_d t}$ and the initial condition $C = 0$ everywhere in the flow region.

Rasmuson et al., (1980) simulated the same problem with the IFD program TRUMP in order to validate the program. The problem considered was subject to the following parameters, considered to be realistic for geologic disposal of high level radioactive wastes: S = 1 m; D_L = 1.35 x 10^{-4} m^2/s; K, volume equilibrium constant = 10^4 m^3/m^3; D_p, diffusivity of rock matrix = 10^{-12} m^2/sec; v_f, velocity of fluid in the fracture = 3 x 10^{-7} m/sec, 2b = 10^{-5} m, and r_0, the radius of the spherical particle = 1.5 m. The decay constant used was λ_d = 2.311 x 10^{-9} $year^{-1}$, corresponding to a half-life of 3 x 10^8 years.

The problem was solved with 25 elements along the fracture with length varying from 15 m (10 elements), 30 m (10 elements) and 100 m (5 elements), and each spherical particle divided 15 concentric elements with Δ_r = 0.1 m. In Fig. 16, the numerical solution obtained with TRUMP for a point in the fracture at Z = 225 m is shown compared with the analytic solution. As can be seen, except for a slightly earlier breakthrough predicted by the numerical solution, the two solutions agree to within 10^{-3} per cent for most of the period simulated.

6. A double-porosity problem. The final illustrative problem is concerned with a fractured system idealized as an equivalent system of two interacting continua. To provide a physical feel for the illustration, we shall consider a system of 10 horizontal fractures, each with a uniform aperture of 10^{-4} m and separated by matrix slabs 1 m in thickness. The aggregate thickness of the rock and fracture is 10 m. If cubic law is assumed, each fracture has an absolute permeability of k_f = 8.333 x 10^{-10} m^2. But if we assume that the

combined effect of the fractures can be replaced by a fracture continuum 10 m thick, then, the equivalent permeability of the fissured continuum amounts to $k_f^* = 8.333 \times 10^{-14}$ m^2. Similarly, if the fracture compressibility is assumed negligible, the specific storage of the fracture continuum is approximately $S_{s,f}^* = 1 \times 10^{-9}$ m^{-1} of water. It is reasonable to assume that the permeability of the matrix may be smaller than k_f^* by one to three orders of magnitude or more, while a value of 10^{-5} m^{-1} is reasonable for the specific storage of the rock, $S_{s,r}$.

Let us now consider the mechanics of fluid transfer between the fissured and the matrix continua. Obviously, in the actual problem, water will drain vertically from the matrix slab upward and downward into adjoining fractures, with the centerline of the slab forming a line of symmetry. If we consider a thin prism of a matrix slab with cross sectional area A, then the amount of water draining from a slab to one adjoining fracture is given by

$$Q_{f,r} = \frac{k_r \rho g}{\mu} \cdot A \cdot \frac{\psi_r - \psi_f}{D_{f,r}} \tag{38}$$

$$= \frac{k_r \rho g}{\mu} \alpha^* (\psi_r - \psi_f) \tag{39}$$

where $\alpha^* = A/D_{f,r}$ and $D_{f,r} = 0.5$ m. Now since each slab is doubly-draining, the actual volume of water transfer from a given prism of the matrix continuum of thickness H to the prism of fracture continuum at the same location is 20 times $Q_{f,r}$ and is equal to $(k_r \rho g/\mu)(20\alpha^*)(\psi_r - \psi_f)$.

It is of interest here to compare α^* with the geometric parameter often used to quantify the coupling term in the differential expression of the double-porosity model. For this, consider a prism of each medium at the same location, with cross sectional area A and height H, where H is the thickness of the media. Then, if we normalize α^* with reference to bulk volume, we get a volume-normalized parameter related to α. That is, α has a dimension of reciprocal area and in the present case, α is related 1/(S)(H).

In order to solve this interacting-continua problem using TERZAGI, a problem that has been studied by Barenblatt et al (1960), Warren and Root (1963), Odeh (1965), and many others, was chosen. The problem involves a well piercing the fractured-continuum that is areally infinite. The well is produced at a constant rate Q. As has been done by Warren and Root (1963), this problem can be analyzed in terms of four dimensionless groups,

$$T^*_{D_f} = \frac{k^*_f \rho g t}{S^*_{s,f} \mu r_w^2} \tag{40}$$

$$P^*_{D_f} = \frac{2\pi k^*_f \rho g \Delta\psi}{Q\mu} \tag{41}$$

$$\lambda = \alpha r_w^2 \frac{k_r}{k^*_f} \tag{42}$$

and

$$\omega = \frac{S^*_{s,f}}{S^*_{s,f} + S_{s,r}} \tag{43}$$

The problem, involving 10 uniformly spaced fractures was studied using TERZAGI. A number of runs were made to study the effect of varying λ, ω, and the magnitude of wellbore storage capacity. In addition, one run was made with spatially varying k_f^* to consider "skin" effect near wellbore as well as increased fracture intensity beyond about 110 m from the well axis. The results are summarized in three double-logarithmic plots, Figs. 17, 18, and 19.

In Fig. 17 the double porosity results are compared with the Theis solution for three values of λ. Increasing λ implies increasing matrix permeability. In the numerical model a 0.1 m radius well was assumed. In order to approximate the line source solution, the well was assumed to be packed-off and hence deriving storativity purely from water compressibility. In one case the well was assumed to have a fluctuating free surface. In the former case, the capacity of the wellbore was assumed to be 10^{-6} m^3 of water per meter of head change while in the latter it was $(0.1)^2\pi$. As can be seen from Fig. 17, the different cases clearly show effects of delayed drainage from the blocks in the range $10^1 < t_{D_f} < 10^6$, when the wellbore storage is small. It is, however, interesting to note that a realistic wellbore radius of 0.1 m with free fluid surface in the well gives a solution which totally masks all the effects that one could hope to see due to variable λ or, equivalently, variable matrix permeability.

Study of the double-porosity system by many workers has showed that the late-time behavior of the system is dominated by the combined storativities of the matrix and the fractured media while the intermediate-time behavior is influenced by ω, the ratio of the fissure storativity to matrix storativity. In

Fig. 18, two cases are compared, $\omega = 10^{-4}$ and $\omega = 10^{-2}$. As should be expected, the late-time solutions for these two cases are distinct from each other.

The final case shown in Fig. 19 was actually chosen to illustrate the generality of the numerical approach over the analytical approach. In a general integral, numerical model, the system is described as a complex of several isolated continua, each interacting with the other. Insofar as the numerical approach is concerned, the double-porosity problem is a simplified special case which can be handled with ease. The case considered in Fig. 19 considers the fissure-continuum to have radially varying k_f^*, to simulate the existence of a low-permeability skin close to the well and to account for increased permeability due to fracturing beyond about 100 m from the well.

As can be seen from Fig. 19, the presence of the low-permeability skin causes much higher drawdowns than the $\lambda = 2 \times 10^{-5}$ case, after $t_{D_f} \sim 10^2$. For $r < 100$ m, the two cases have identical parameters except for the skin. Detailed study of the printouts showed that the pressure transient extended beyond about 100 m for $t_{D_f} > 10^{10}$. As a result, the variable k_f^* flattens markedly after that time and eventually crosses the $\lambda = 2 \times 10^{-5}$ curve at $t_{D_f} \sim 10^{12}$.

CONCLUSIONS

The Integral Finite Difference Method (IFDM) combines the power of an integral formulation with the simplicity of finite-difference gradients to constitute a powerful tool for simulating fluid flow in a variety of fractured rock systems. The conventional finite-difference method is a subset of

IFDM and is included in it as a limiting case. The principal difference between the IFDM and the Finite-Element Method (FEM) lies in the ability of the latter to facilitate generalized gradient evaluations. A unique feature of the IFDM is that the information required to generate conductances between communicating volume elements are handled as input in a simple fashion. This feature provides unique advantages in handling heterogeneous systems such as fractured porous media with sharply-varying material properties.

Insofar as simulating fluid flow in fractured systems is concerned, we do possess fairly sophisticated abilities. The chief problem that now confronts us is that of obtaining the relevant data from the field to provide input to the computational model. The information required to be handled for characterizing all the discrete fractures of even a small system is too voluminous and difficult to obtain. To minimize this problem one may desire to replace the discrete system with an equivalent macroscopically average system. While such equivalent systems are conceptually interesting, they have two disadvantages when one desires to utilize them in situations where a high degree of certainty is desired (e.g., radioactive waste isolation). The first is that very little is known as yet about the quantitative relationships that exist between the small- and large-scale parameters. Secondly, by their very nature, the macroscopic parameters possess inherent uncertainty or imprecision about them. This may suggest that these parameters cannot be expected to answer questions beyond a certain level of accuracy. In regard to waste isolation, the required degree of precision may be finer than the uncertainties associated with the macroscopic parameters.

ACKNOWLEDGEMENTS

In obtaining the various results presented in this paper, I have had many interesting discussions with the following colleagues to whom my sincere thanks are due: G. Bodvarsson, S. Juprasert, W. A. Palen, A. Rasmuson, and J. S. Y. Wang. I would also like to thank Jahan Noorishad and Karsten Pruess for constructive criticisms of the manuscript.

This work was supported by the Assistant Secretary for Resource Applications, Office of Industrial and Utility Applications and Operations, Geothermal Energy Division of the U. S. Department of Energy under Contract W-7405-ENG-48.

NOMENCLATURE

$a_{v,f}$	coefficient of compressibility for a fracture	$[LT^2/M]$
A_f	area of interface between fracture and matrix elements	$[L^2]$
$A_{\ell m}$	coefficients of the conductance matrix	[M/LT]
b	one-half of the fracture aperture	[L]
B_ℓ	known quantity including sources and boundary conditions	[M/T]
C	chemical concentration	
C_r	dimensionless coefficient characterizing permeability contrast between fracture and rock matrix	
$d_{\ell,i}$, $d_{m,i}$	distance between nodal point ℓ or m to the interface between them	[L]
D_L	longitudinal dispersion coefficient	$[L^2/T]$
D_p	diffusivity of solute in rock matrix	$[L^2/T]$
$D_{\ell m}$	distance between nodal points ℓ and m	[L]
e	void ratio	
e_f	void ratio of a fracture	
g	acceleration due to gravity	$[L/T^2]$
g_ℓ	rate of fluid production per unit volume	$[M/L^3T]$
G_ℓ	rate of fluid generation from volume element ℓ	[M/T]
h, H	thickness of flow region	[L]
I	number of fractures	
K	volume equilibrium constant in the chemical transport problems	$[L^3/L^3]$
K	hydraulic conductivity	[L/T]
K_j, K_r	hydraulic conductivity of fracture or rock matrix	[L/T]

K_f^*, K_r^*	hydraulic conductivity of fracture continuum or matrix continuum	[L/T]
$K_{f,r}$	hydraulic conductivity of the fracture rock interface	[L/T]
$\Delta\ell_f$	length of fracture trace on the plane across which flow is measured	[L]
$m_{c,\ell}$	specific fluid mass capacity of material in element ℓ	$[M/L^3L]$
m_v	coefficient of volume change	$[LT^2/M]$
$m_{v,f}$	coefficient of volume change for a fracture	$[LT^2/M]$
$M_{w,\ell}$	mass of water in element ℓ	[M]
$M^o_{w,\ell}$	mass of water in element ℓ at t = 0	[M]
$M_{c,\ell}$	fluid mass capacity of element ℓ	[M/L]
n	porosity	
n_f	porosity of a fracture	
P_D	dimensionless pressure	
Q	volumetric fluid flux rate	$[L^3/T]$
Q_f	volumetric flux across a fracture surface	$[L^3/T]$
r_f	fracture radius	[L]
r_w	radius of well	[L]
S	fracture spacing	[L]
S_s	specific storage	$[L^3/L^3L]$
$S_{s,\ell}$	specific storage of material in element ℓ	$[L^3/L^3L]$
$S_{s,f}$, $S_{s,r}$	specific storage for fracture and rock, respectively	$[L^3/L^3L]$
$S^*_{s,f}$, $S^*_{s,r}$	specific storage for fracture continuum and rock continuum, respectively	$[L^3/L^3L]$
t_o	initial time	[T]
$\Delta t_{stab,\ell}$	stable time step for volume element ℓ	[T]

t_{D_f}, T_{D_f}	dimensionless time	
U	conductance of a surface segment	[M/LT]
U_{ℓ}	conductance of an exterior surface segment between elements ℓ and b	[M/LT]
$U_{\ell,m}$	conductance of an interior surface segment between elements ℓ and m	[M/LT]
v_f	velocity of fluid in fracture	[L/T]
V	volume	$[L^3]$
V_{ℓ}	volume of element ℓ	$[L^3]$
V_s	volume of solids	$[L^3]$
V_v	volume of voids	$[L^3]$
V_f^*, V_r^*	volume of fracture continuum or rock continuum element	$[L^3]$
$V_{b,f}$	bulk volume of fracture	$[L^3]$
$V_{s,f}$	volume of solids associated with a fracture element	$[L^3]$
$V_{v,f}$	void volume of a fracture element	$[L^3]$
w	fracture width (= 2b)	[L]
z	elevation	[L]
Z	axis of flow in chemical transport problem	[L]
α	coefficient coupling the fracture continuum and the rock continuum and the rock continuum in the eifferential equation	$[1/L^2]$
α^*	coupling coefficient between the fracture and matrix continua in the integral formulation	[L]
β	coefficient of bulk compressibility for water	$[LT^2/M]$
Γ	surface bounding a volume element	$[L^2]$
$\Delta\Gamma_{f,r}$	surface segment separating fracture and rock	$[L^2]$

$\Delta\Gamma_{\ell,m}$, $\Delta\Gamma_{\ell,b}$	surface separating two interior elements ℓ and m or an interior element P and boundary element b	$[L^2]$
$d\Gamma$	small surface segment	$[L^2]$
λ	an implicit weighting factor; also a dimensionless coefficient in double porosity simulation	
λ_d	decay coefficient	[1/T]
μ	coefficient of viscosity	[M/LT]
ρ	density of fluid	$[M/L^3]$
ρ_ℓ	density of fluid in element ℓ	$[M/L^3]$
$\rho_{\ell b}$ $\rho_{\ell m}$	density of fluid at interface between elements ℓ and b or elements P and m	$[M/L^3]$
ϕ	hydraulic head or fluid potential	[L]
φ_b	potential at the boundary	[L]
φ_ℓ	average of potential over element ℓ	[L]
ϕ_r	average potential in a matrix block	[L]
ϕ°_ℓ, ϕ°_m	initial values of ϕ_ℓ and ϕ_m at t = 0	[L]
Ψ_ℓ	pressure head over element ℓ	[L]
$\bar{\Psi}_\ell$	average value pf Ψ_ℓ over ℓ	[L]
ω	dimensionless variable	

REFERENCES

Barenblatt, G. E., I. P. Zheltov, and I. N. Kochina, "Basic concepts in the theory of homogeneous liquids in fissured rocks." J. Appl. Math (USSR) 24(5), 1286-1303, 1960.

Cinco-Ley, H., F. Samaniego, and N. Dominguez, "Transient behavior for a well with a finite conductivity vertical fracture. Paper SPE 6014, 51 Annual Meeting, Soc. Pet. Eng. AIME, 1976.

Dusinberre, G. M., Heat transfer calculations by finite differences. Int'l Text Book Co., Scranton, Pennsylvania, 1961.

Edwards, A. L., "TRUMP: A computer program for transient and steady state temperature distributions in multidimensional systems." Rept. UCRL 14754, Revision III, National Technical Information Service, Springfield, VA., 1972.

Gringarten, A. C. and H. J. Ramey, Jr., "Unsteady-state pressure distributions created with a single horizontal fracture, partial penetration or restricted entry." Soc. Pet. Eng. J., Aug. 1977, 413-426.

Haimson, B. and Fairhurst, C., "In situ stress determination at great depth by means of hydraulic fracturing." in Rock Mechanics: Theory and Practice, Proc. Eleventh Intl. Symp. on Rock Mech., W. H. Somerton, ed., 1970.

Lippmann, M. J., C. F. Tsang, and P. A. Witherspoon, "Analysis of the response of geothermal reservoirs under injection and production procedures, Paper No. SPE 6537, Soc. Pet. Eng. AIME, 47th Calif. Annual Meeting, Bakersfield, Calif., 1977.

MacNeal, R. H., "An asymmetrical finite difference network." Quart. Appl. Math., 11, 295-310, 1953.

Narasimhan, T. N. and W. A. Palen, "A purely numerical approach for analyzing flow to a well intercepting a vertical fracture." Preprint No. 7983, Soc. Pet. Eng. AIME, California Regional Meeting, Ventura, April, 1979.

Narasimhan, T. N. and P. A. Witherspoon, "An integrated finite-difference method for analyzing fluid flow in porous media." Water Resources Res., 12(1), 57-643, 1976.

Narasimhan, T. N., P. A. Witherspoon, and A. L. Edwards. "Numerical model for saturated-unsaturated flor in deformable porous media, Part 2: the algorithm." Water Resources Res., 14(2), 255-261, 1978.

Neuman, S. P. and T. N. Narasimhan, "Mixed explicit-implicit iterative finite element method for diffusion-type problems, Part I. Theory." Int. J. Num. Meth. in Eng. 11, 309-323, 1977.

Odeh, A. S., "Unsteady behavior of naturally fractured reservoirs." Soc. Pet.Eng. J., Sept. 1965, 245-

Palen, W. A., "The roles of fluid pressure and fluid flow in the hydraulic fracturing process." Ph.D. dissertation, Dept. of Mechanical Eng., Univ. of California, Berkeley, June 1980.

Pruess, K., and R. C. Schroeder, SHAFT79, User's Manual, Rept. LBL-10861, Lawrence Berkeley Laboratory, Berkeley, California, March 1980.

Rasmuson, A., T. N. Narasimhan, and I. Neretnieks, "Chemical transport in a fissured rock: validation of a numerical model." Manuscript in preparation.

Rasmuson A. and I. Neretnieks, "Exact solution of a model for diffusion in particles and longitudinal dispersion in packed beds." Am Inst. Chem. Eng. J., in press, 1980.

Wang, J. S. Y., T. N. Narasimhan, C. F. Tsang, and P. A. Witherspoon, "Transient flow in tight fractures." Proc. Invitational Well Testing Symposium, Report No. LBL-7027, Lawrence Berkeley Laboratory, Berkeley, California, pp. 103-116, 1977.

Warren, J. E. and P. J. Root, "The behavior of naturally fractured reservoirs." Soc. Pet. Eng. J., Sept. 1963, 245-255.

Witherspoon, P. A., J. S. Y. Wang, K. Iwai, and J. E. Gale, "Validity of cubic law for fluid flow in a deformable rock fracture." Water Resources Res., 1980 (in press).

LIST OF FIGURES

Fig. 13. Simulation of hydraulic fracturing: field data on injection rate and pressure (after Palen, 1980). (XBL 807-3481)

Fig. 14. Simulation of hydraulic fracturing: comparison of numerical results and field observations (after Palen, 1980). (XBL 807-3479)

Fig. 15. Chemical transport in a fissured medium: problem description (after Rasmuson et al. 1980). (XBL-8010-2956)

Fig. 16. Chemical transport in a fissured rock: comparison of numerical and analytical results. (XBL 809-2840)

Fig. 17. Simulation of a double-porosity medium: effect of varying λ. (XBL 8010-2849)

Fig. 18. Simulation of flow in a double-porosity medium: effect of varying ω. (XBL 8010-2848)

Fig. 19. Simulation of a double-porosity medium: effect of spatially varying permeability. (XBL 8010-2847)

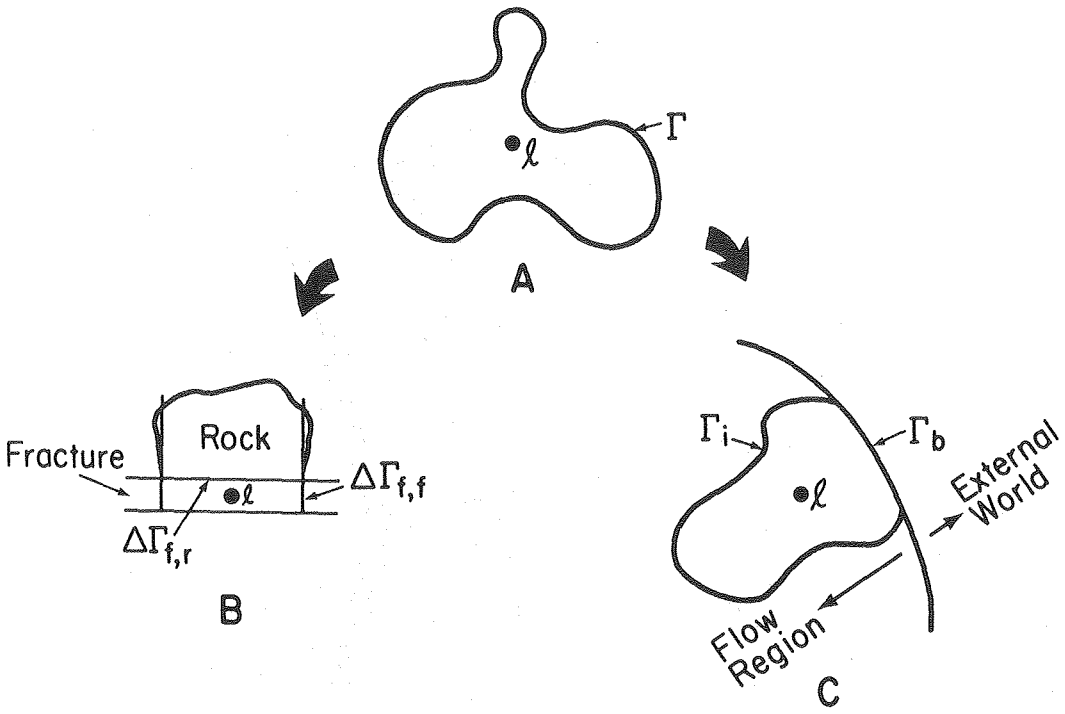

Fig. 1. Examples of volume elements, nodal points, and bounding surfaces. (XBL 807-7236)

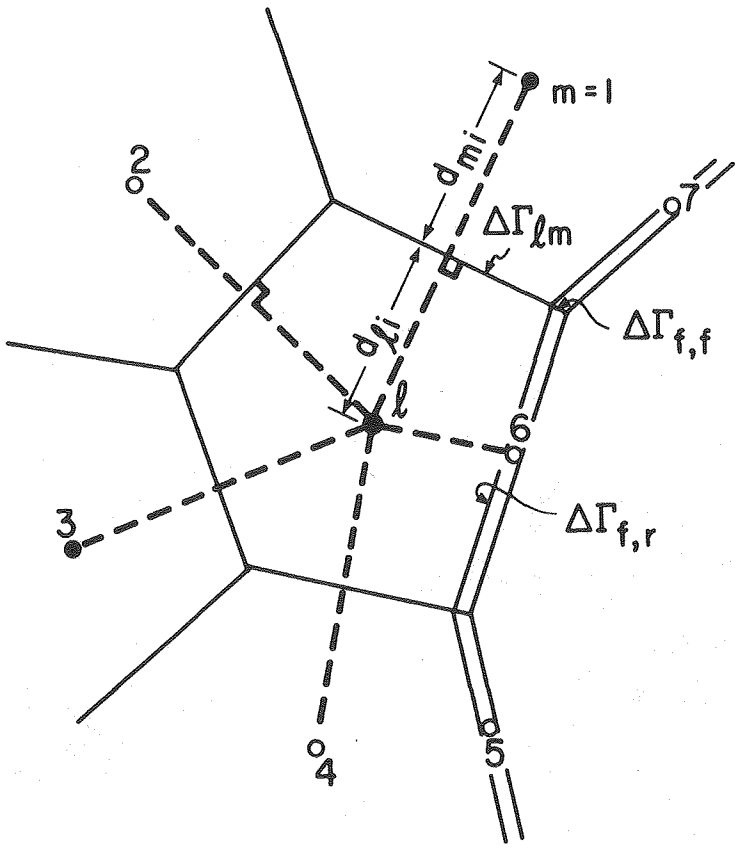

Fig. 2. Philosophy of mesh discretization for the Integral Finite Difference Method. (XBL 807-7234)

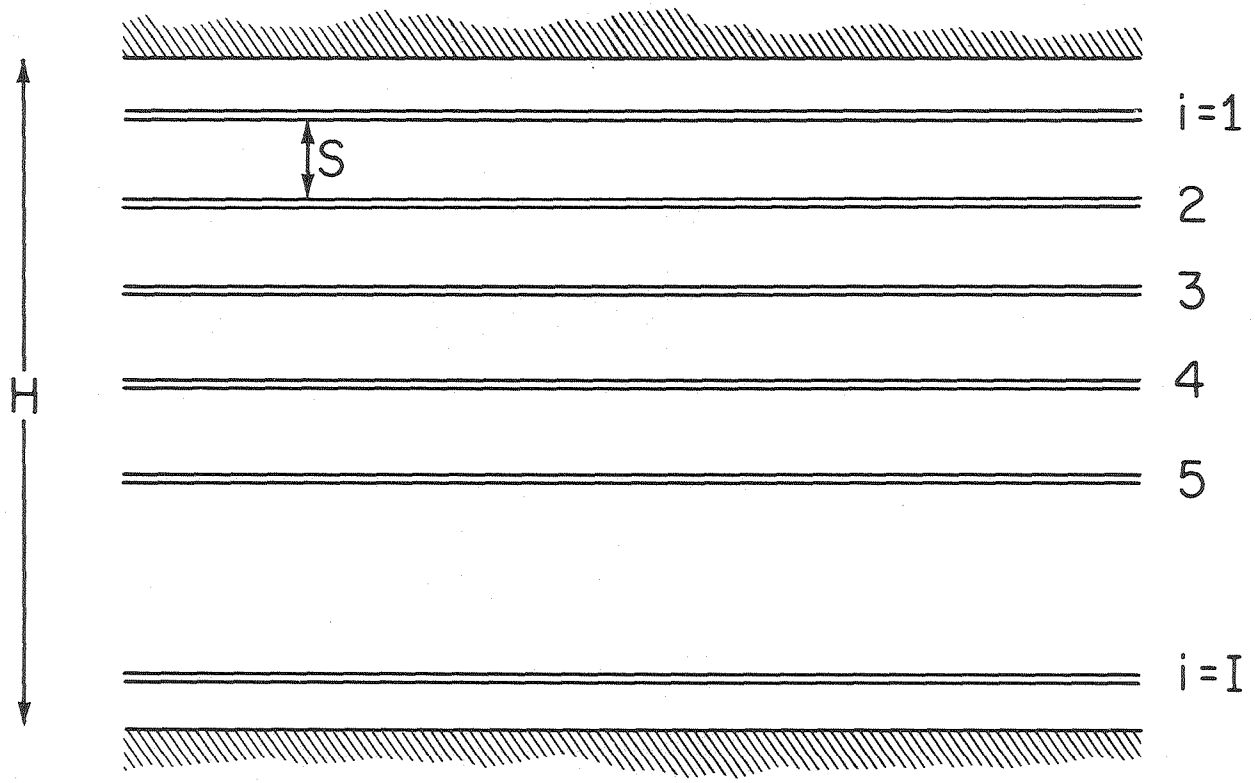

Fig. 3. System of horizontal fractures in a permeable medium. (XBL 809-2844)

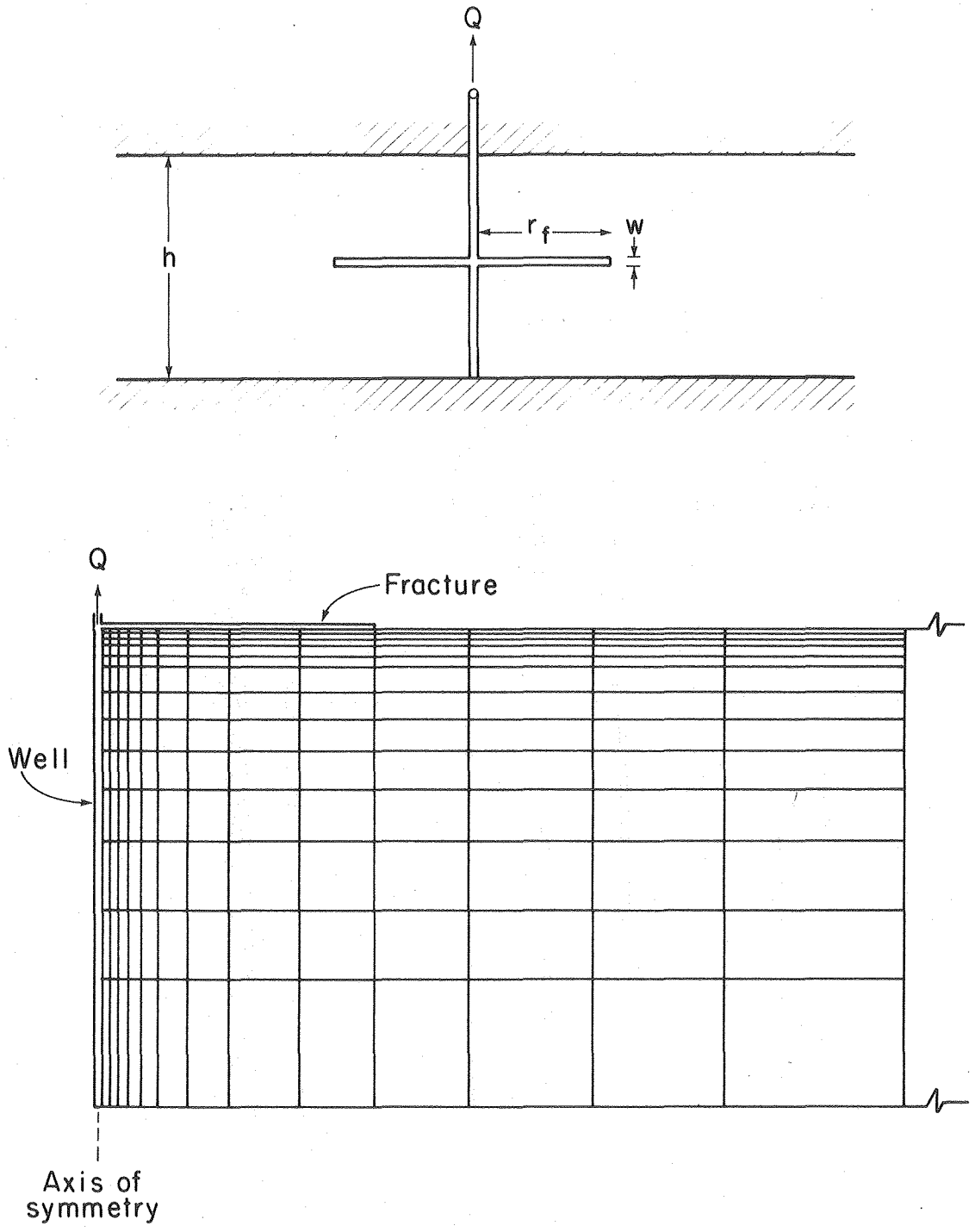

Fig. 4. Single horizontal fracture in permeable rock: problem description. (XBL 804-7003)

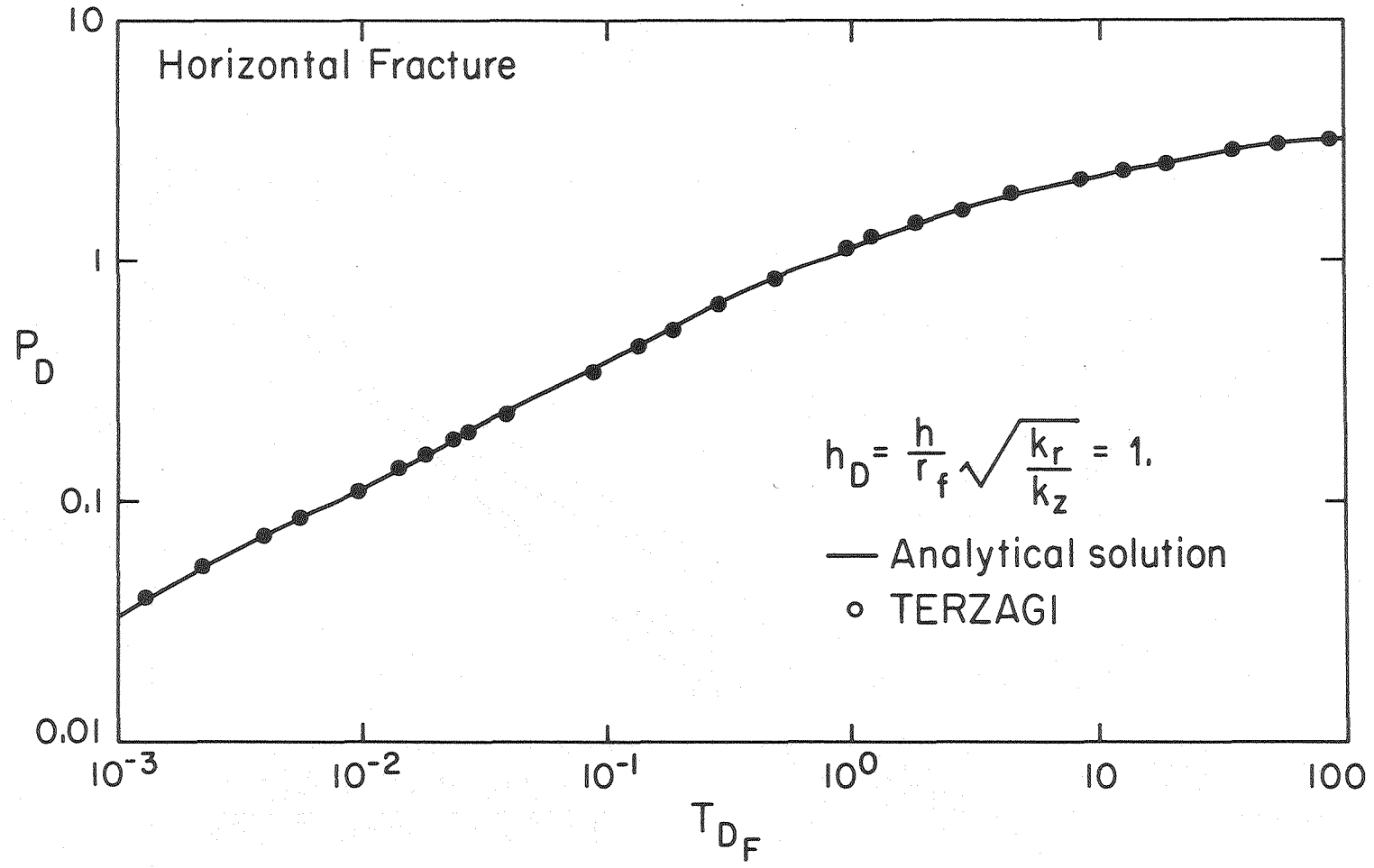

Fig. 5. Horizontal fracture problem: comparison of analytical and numerical results. (XBL 809-2843)

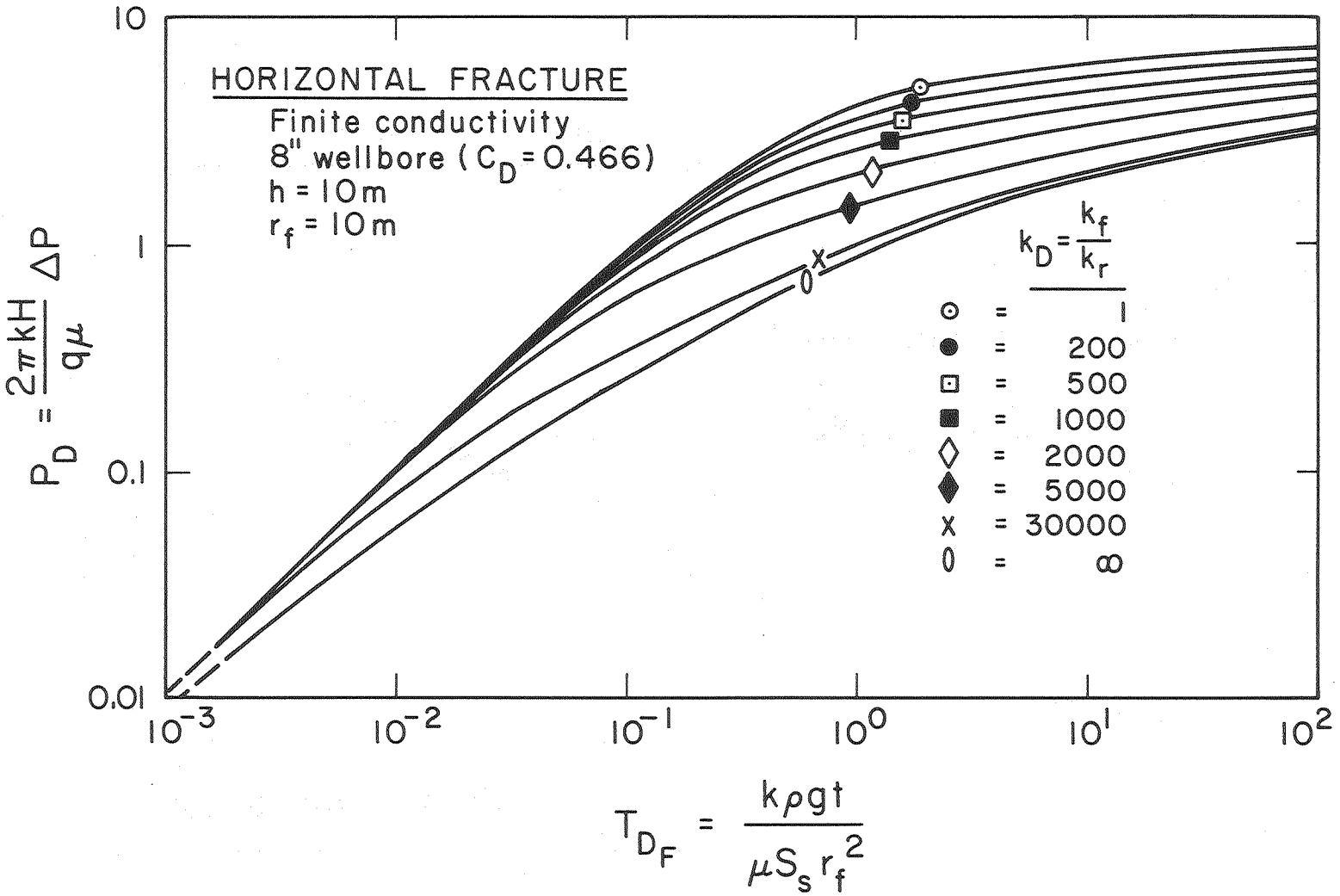

Fig. 6. Horizontal fracture problem: type curves for finite fracture conductivity (after Bodvarsson and Narasimhan, 1981). (XBL 804-6897)

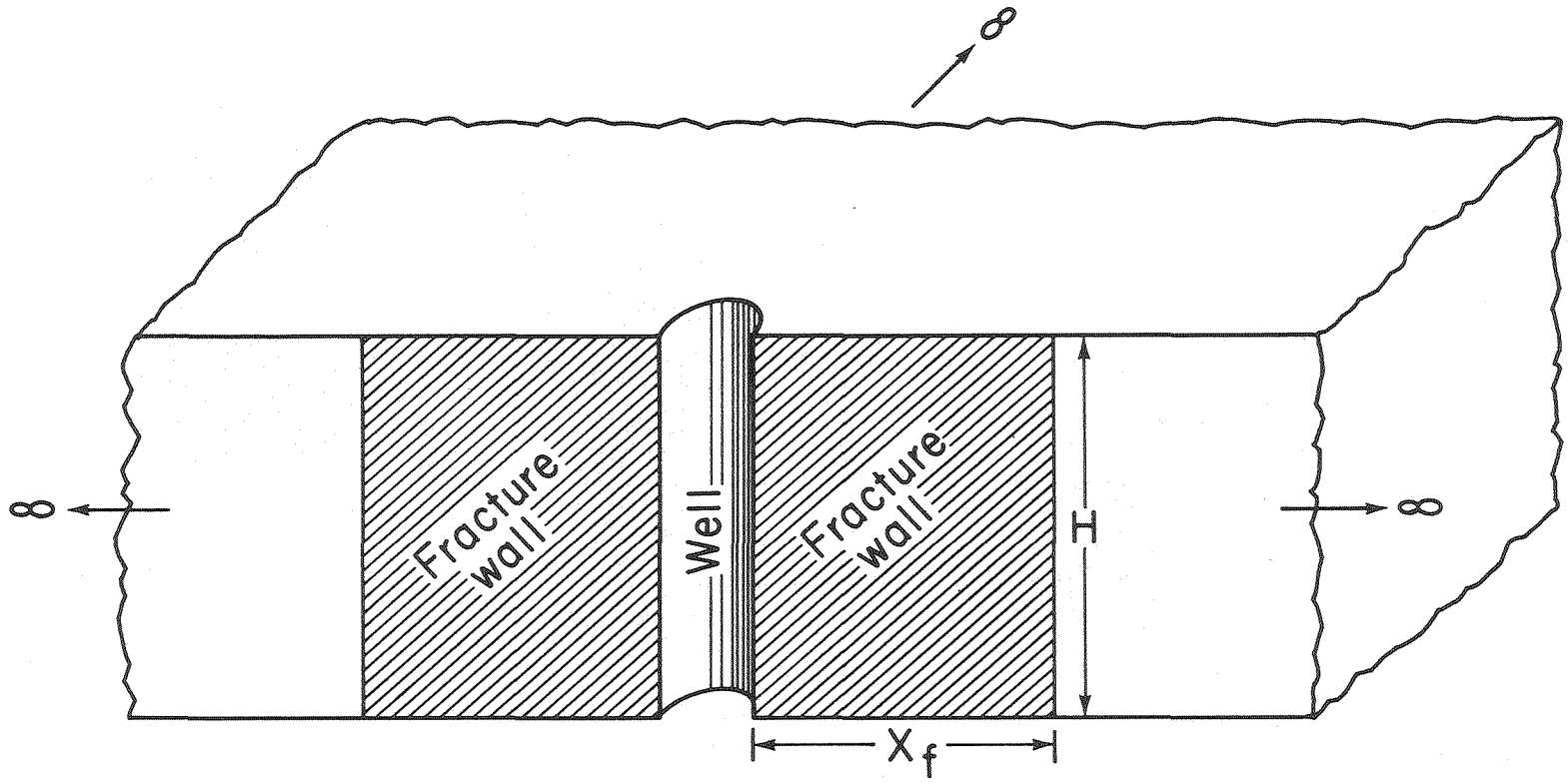

Fig. 7. Single vertical fracture in permeable rock: problem description. (XBL 809-2845)

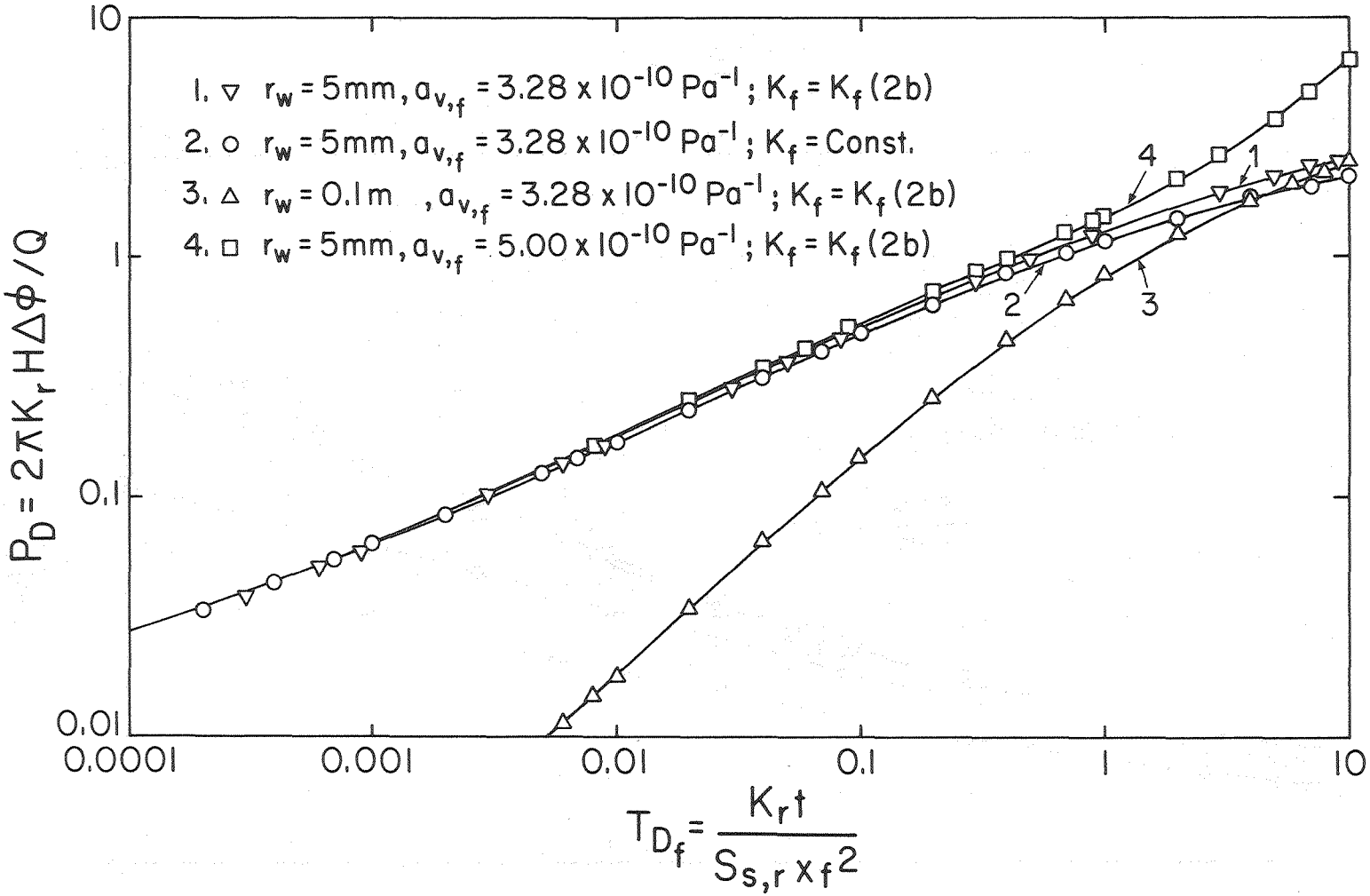

Fig. 10. Vertical fracture problem: effect of fracture deformation. (XBL 809-2841)

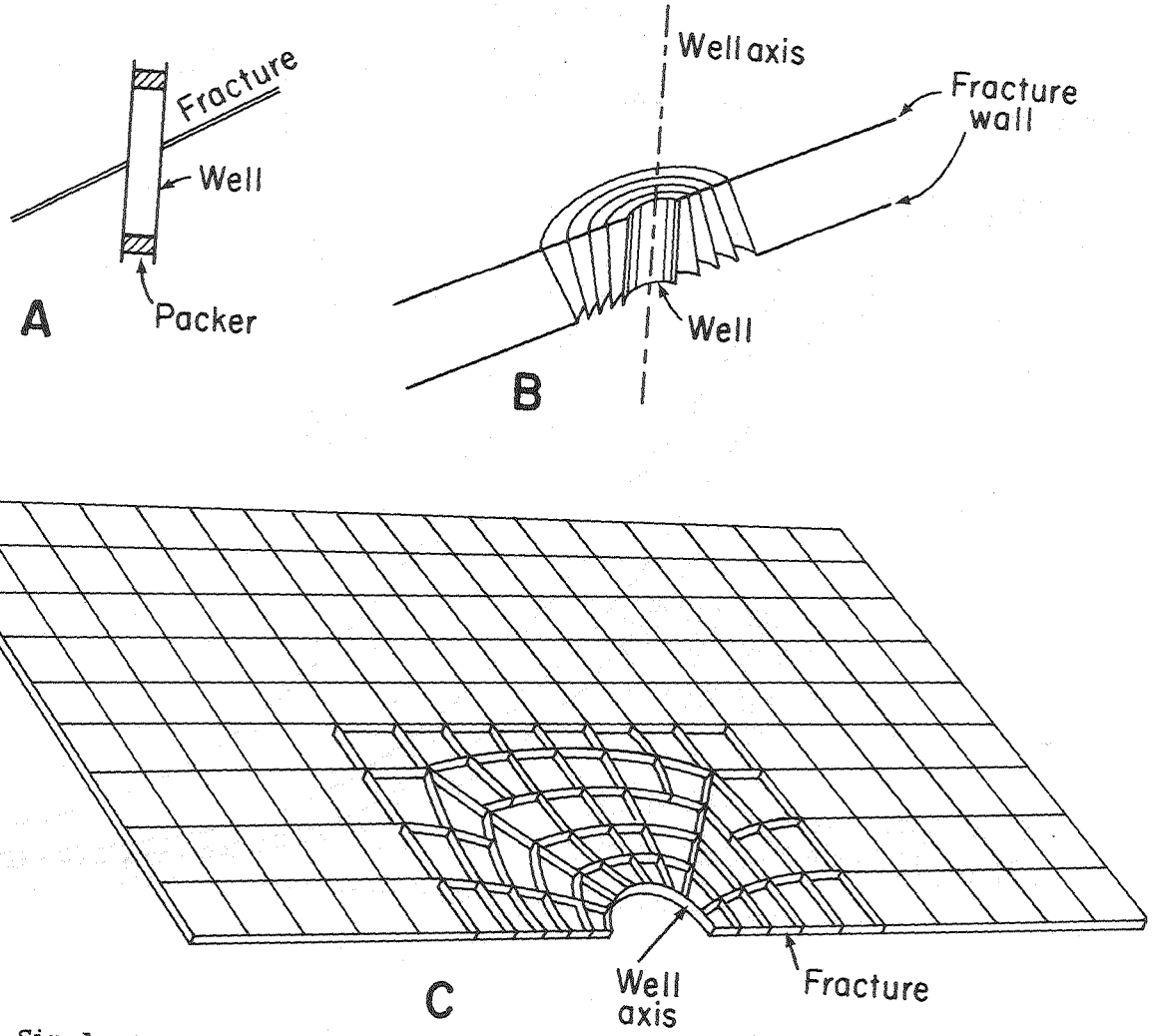

Fig. 11. Single inclined fracture in a permeable medium: problem description (Juprasert, personal communication). (XBL 810-2846)

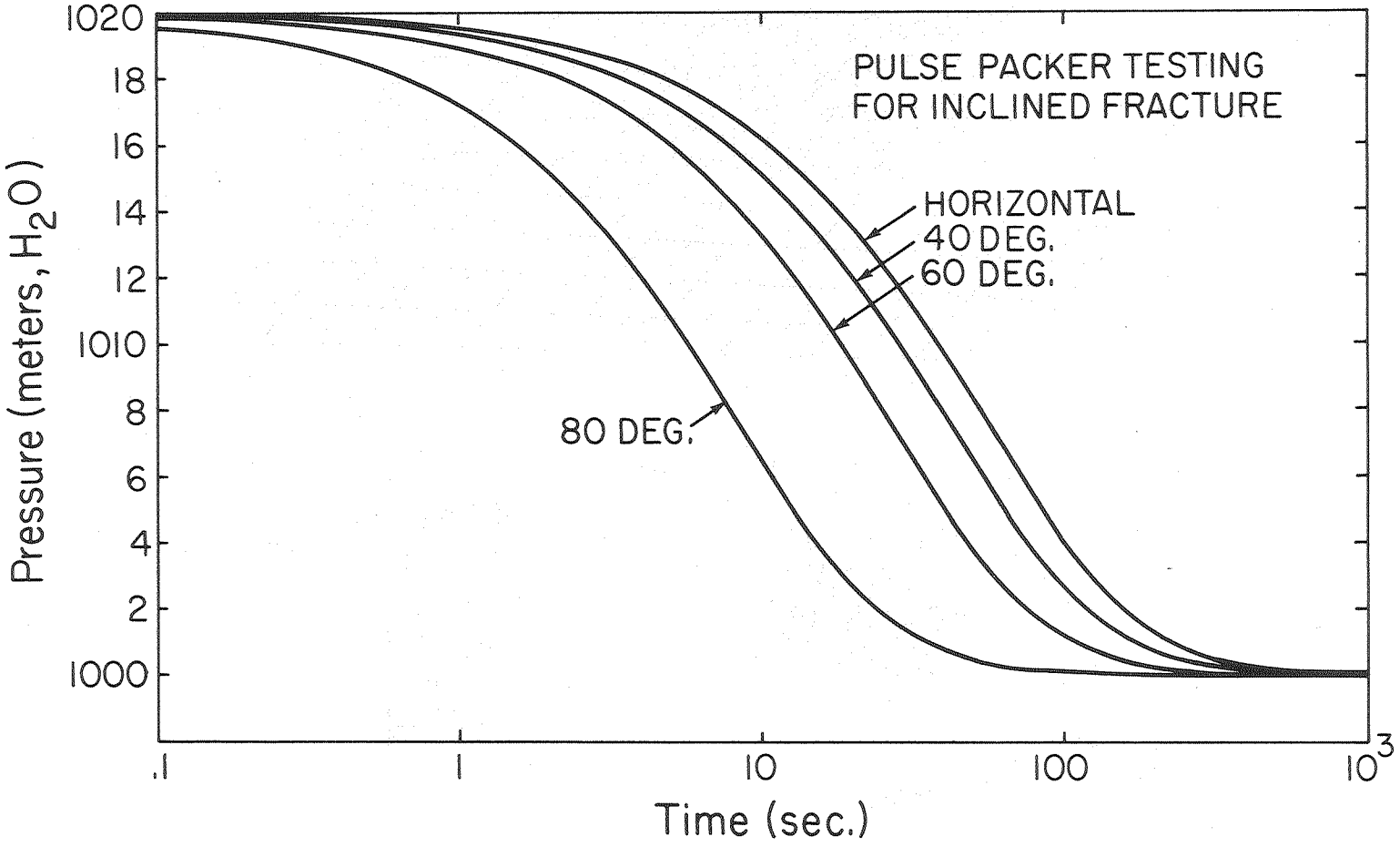

Fig. 12. Inclined fracture problem: solutions for various inclinations (Juprasert, personal communication). (XBL 809-2842)

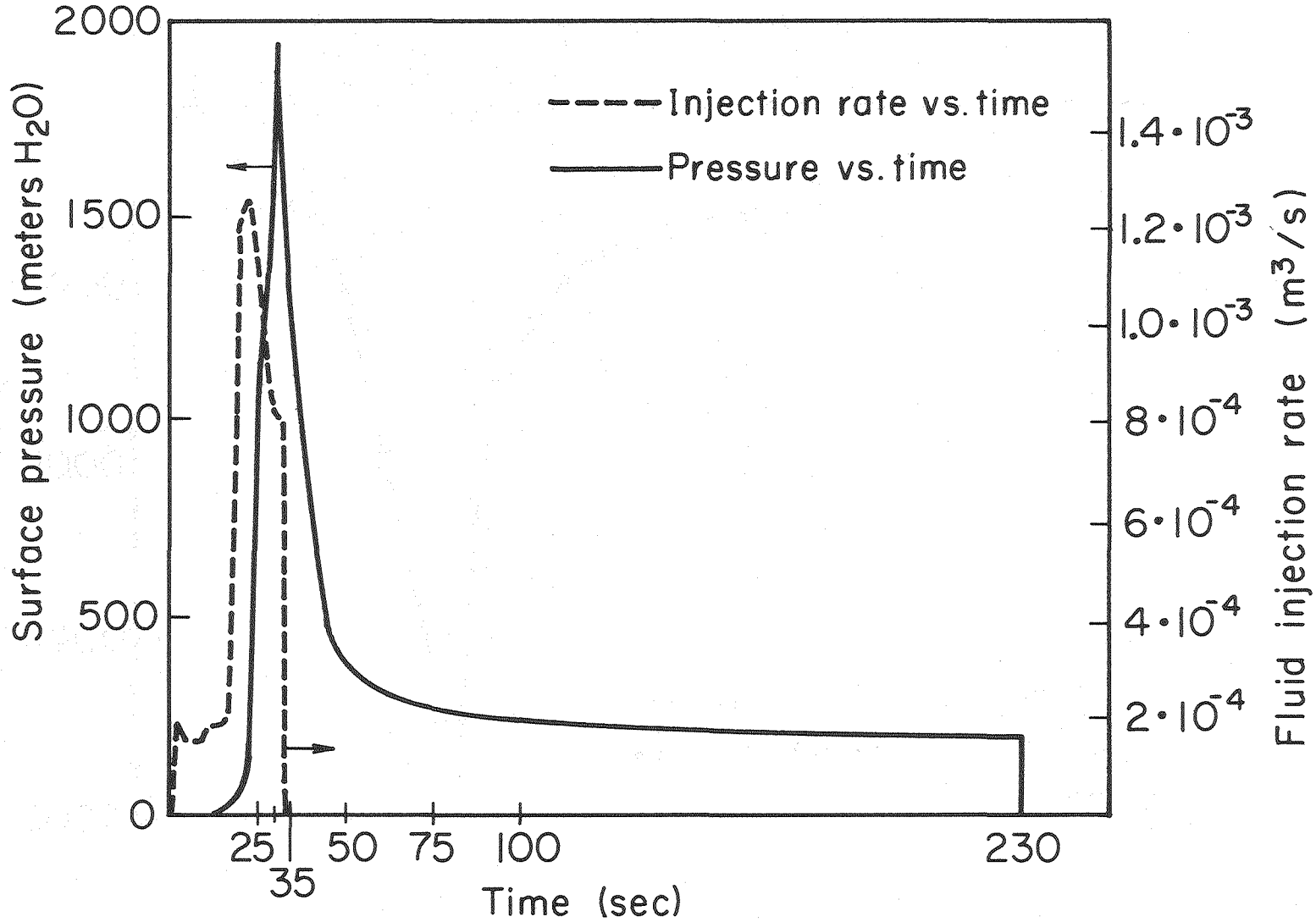

Fig. 13. Simulation of hydraulic fracturing: field data on injection rate and pressure (after Palen, 1980). (XBL 807-3481)

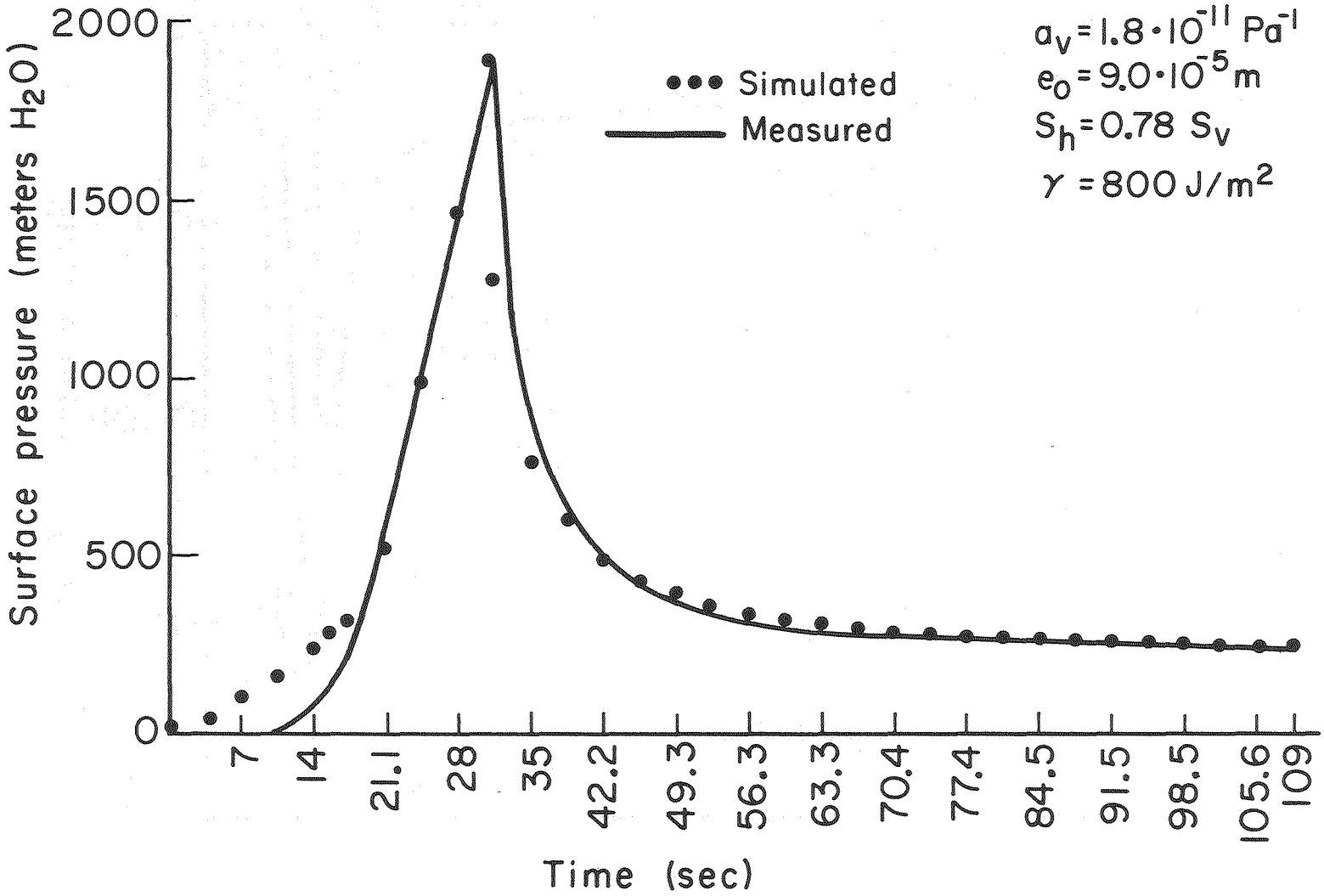

Fig. 14. Simulation of hydraulic fracturing: comparison of numerical results and field observations (after Palen, 1980). (XBL 807-3479)

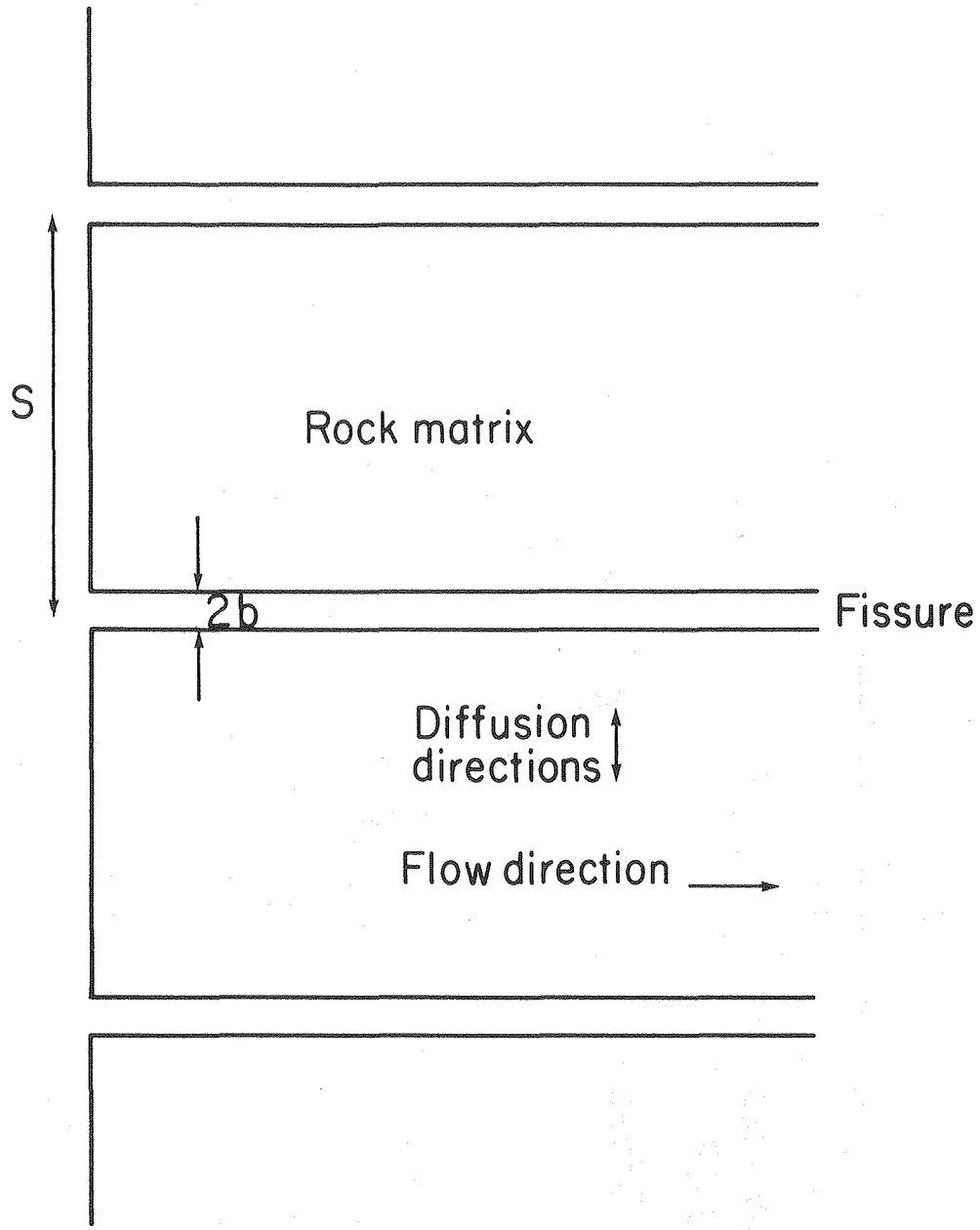

Fig. 15. Chemical transport in a fissured medium: problem description (after Rasmuson et al. 1980). (XBL-8010-2956)

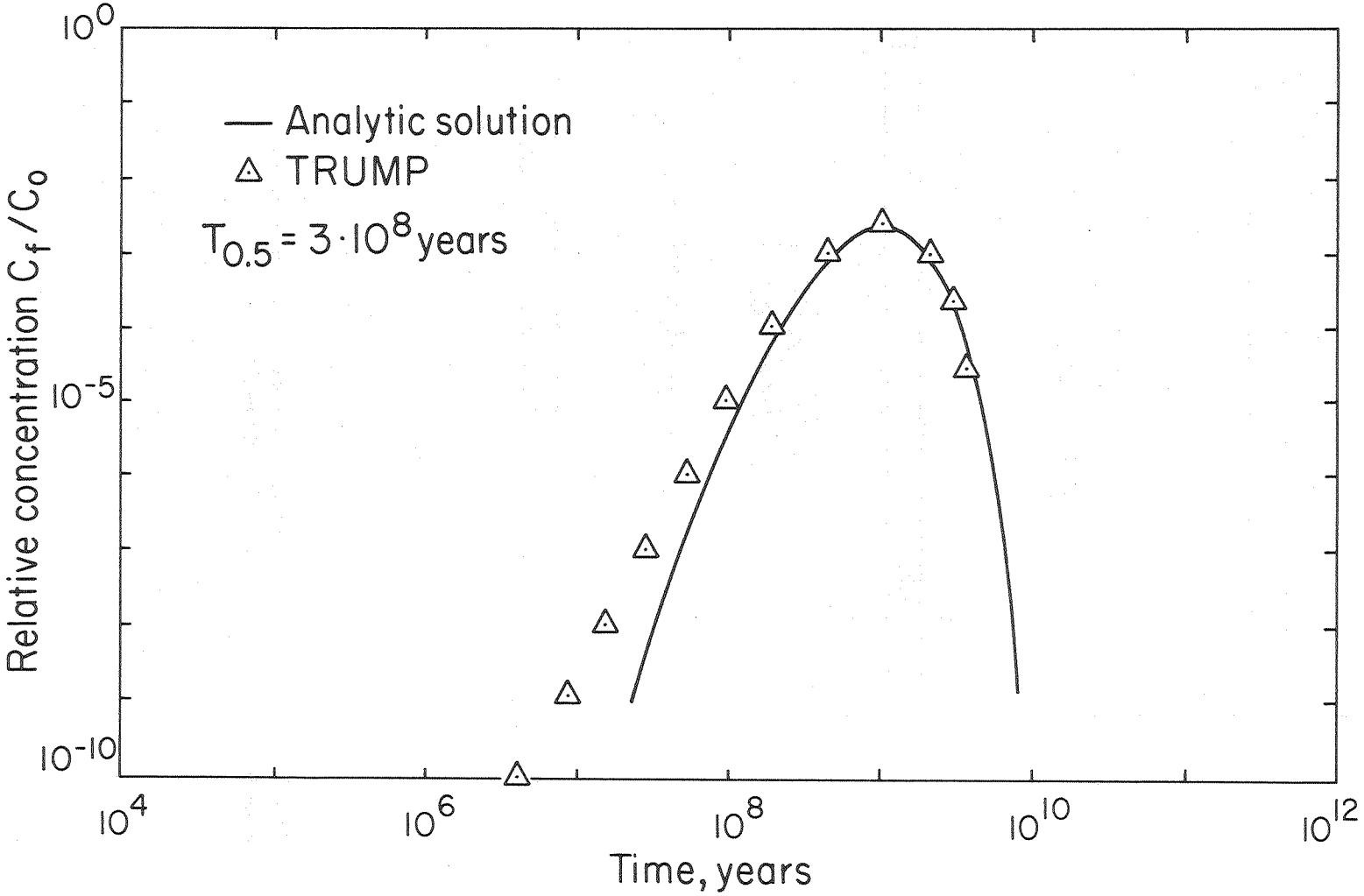

Fig. 16. Chemical transport in a fissured rock: comparison of numerical and analytical results. (XBL 809-2840)

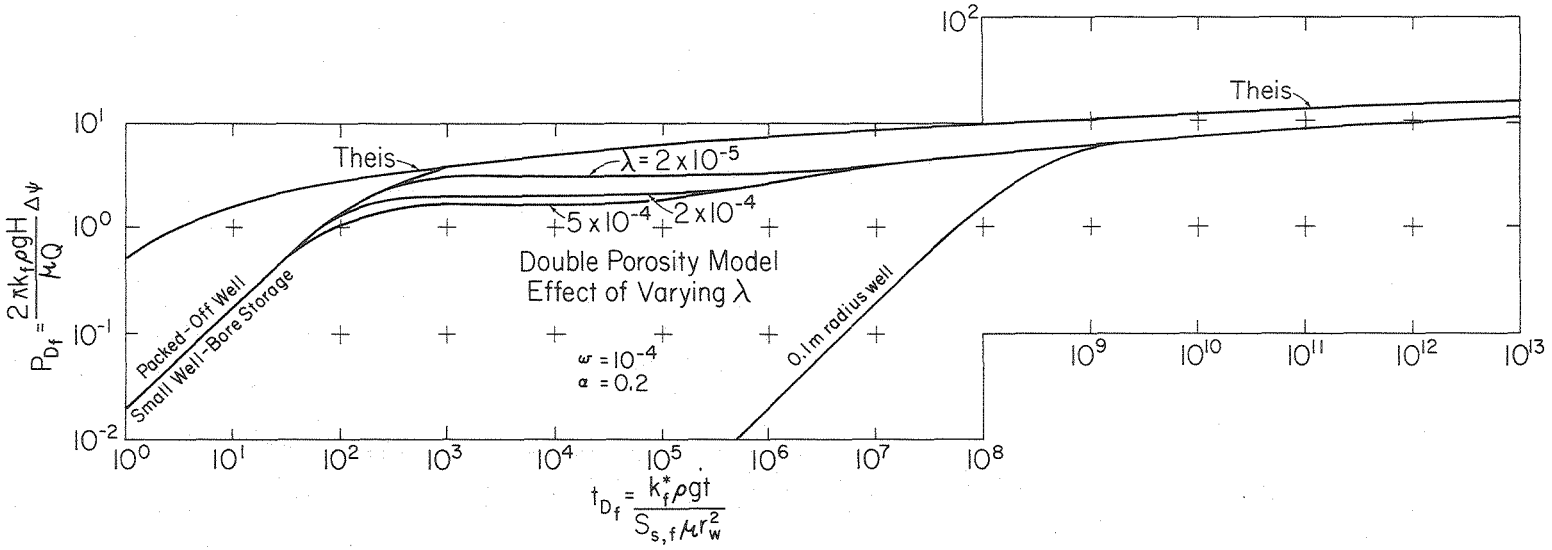

Fig. 17. Simulation of a double-porosity medium: effect of varying λ. (XBL 8010-2849)

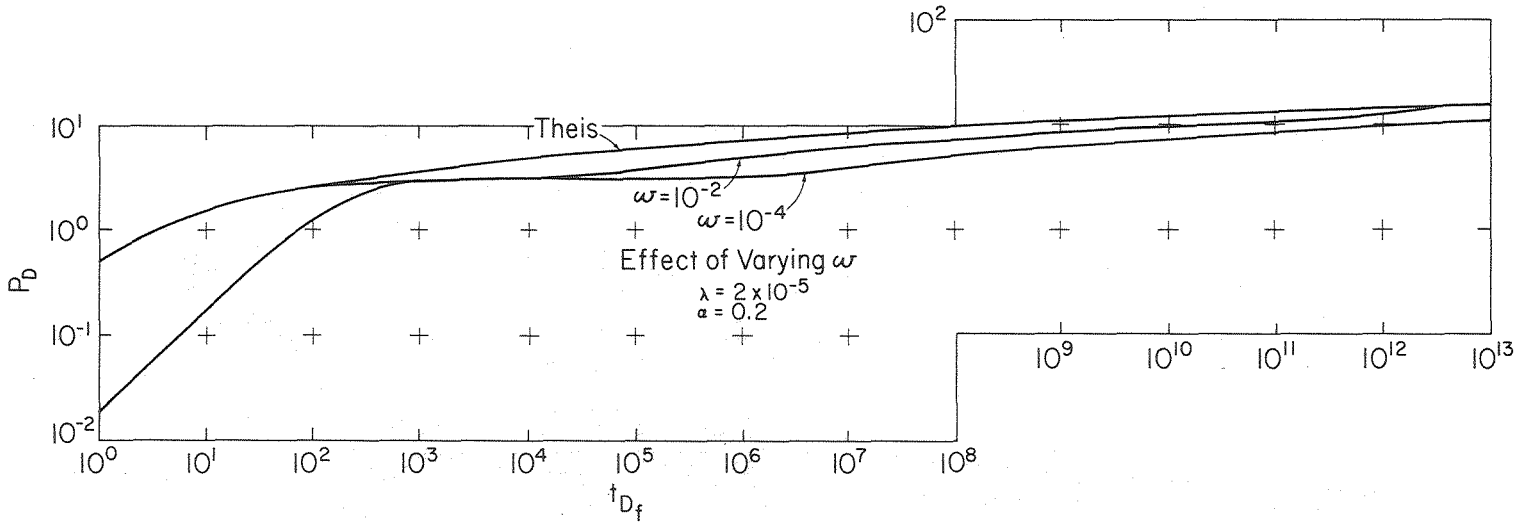

Fig. 18. Simulation of flow in a double-porosity medium: effect of varying ω. (XBL 8010-2848)

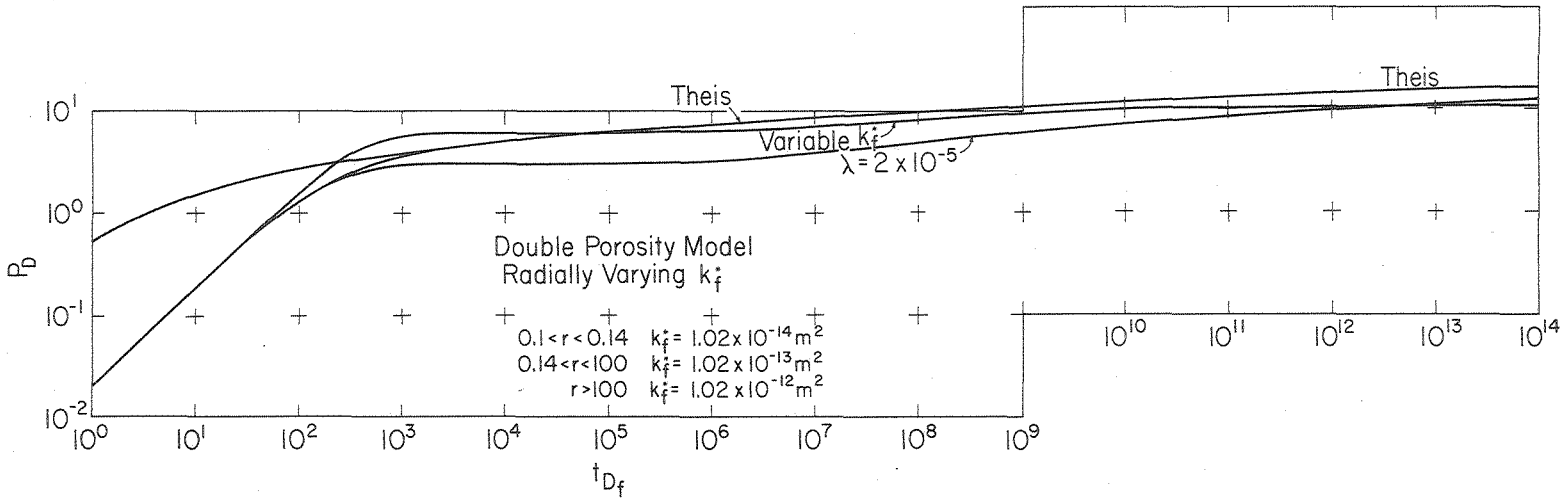

Fig. 19. Simulation of a double-porosity medium: effect of spatially varying permeability. (XBL 8010-2847)